Journal of Soft Computing in Civil Engineering 7-3 (2023) 68-110

Contents lists available at SCCE

Journal of Soft Computing in Civil Engineering

Journal homepage: www.jsoftcivil.com

Prediction of Compressive Strength for Fly Ash-Based Concrete: Critical Comparison of Machine Learning Algorithms

Sifti Wadhawan[1], Akshita Bassi[1], Rajwinder Singh[2], Mahesh Patel[3*]

1. Graduate Students, Department of Civil Engineering, DR BR Ambedkar National Institute of Technology, Jalandhar, Punjab, India
2. Ph.D. Student, Department of Civil Engineering, DR BR Ambedkar National Institute of Technology, Jalandhar, Punjab, India
3. Assistant Professor, Department of Civil Engineering, DR BR Ambedkar National Institute of Technology, Jalandhar, Punjab, India

*Corresponding author: *patelm@nitj.ac.in*

https://doi.org/10.22115/SCCE.2023.353183.1493

ARTICLE INFO

Article history:
Received: 24 July 2022
Revised: 06 February 2023
Accepted: 04 April 2023

Keywords:
Compressive strength;
Fly ash;
Machine learning;
Prediction.

ABSTRACT

In the construction field, compressive strength is one of the most critical parameters of concrete. However, a significant amount of physical effort and natural raw materials are required to produce concrete. In addition, the curing period of concrete for at least 28 days is a must for attaining the required compressive strength. Various types of industrial and agricultural wastes have been used in concrete to reduce cement consumption and problems due to its production. Therefore, considering such constraints, the application of Artificial Intelligence (AI) has been widely used in the current scenarios to predict the desired output parameters. In the present study, 12 input parameters have been considered along with 455 data points and nine Machine Learning (ML) models to forecast the compressive strength of Fly Ash (FA) based concrete. The output from the models has been compared to find the best-fit model in terms of numerous analyses such as visual descriptive statistics, errors, R^2, Taylor's diagram, Feature Importance (FI), and scatter plots. Based on the analysis of the current study, Decision Tree (DT) and Gradient Boost (GB) were found to be the best-fit model because of the least errors and higher R^2 values as compared to other models.

How to cite this article: Wadhawan S, Bassi A, Singh R, Patel M. Prediction of compressive strength for fly ash-based concrete: critical comparison of machine learning algorithms. J Soft Comput Civ Eng 2023;7(3):68–110. https://doi.org/10.22115/scce.2023.353183.1493

1. Introduction

In the past few years, the involvement of new technologies, having enormous influence in various sectors, has brought a revolution and significantly impacted human lives [1]. The employment of technology has always benefited people in in primary, secondary or tertiary sectors. However, all these profits and advantages have had an adverse effect on nature. Industries that produce fertilizer, pesticides, chemicals, construction, petroleum and metallurgical products are responsible for the contamination of the surrounding environment. The construction sector contributes 23% of air pollution, 50% of climatic change, 40% of drinking water pollution and 50% of landfill waste [2,3]. In this regard, cement is the binding material used in construction practices as it sets, hardens and adheres to other materials and binds them together firmly. The cement produced in the construction sector is responsible for 5–8% of global CO_2 emissions [4,5]. The cement manufacturing process causes environmental impacts at all stages [5,6]. Annually, 4 billion tons of Portland cement (PC) are produced, and approximately one ton of cement generates 0.8 tons of CO_2 gas [7–9]. This massive amount of carbon dioxide is a severe threat to the environment. In order to overcome this problem, some amount of cement is replaced with alternative pozzolanic materials having similar properties to reduce the hazards problem caused due to cement production. These alternative materials used in the concrete mixture can be sourced from industrial or agricultural sectors [10–13]. Concrete is one of the most used construction materials all over the world as it is known for its high compressive strength, durability, fire resistance, versatility and abrasion resistance. The main objective of designing a concrete mix is determining the amounts of concrete constituents required to form the best mix [14,15]. However, because of miscalculations of mix design, the manufactured concrete can produce low strength. Also, to achieve proper compressive strength, various tests are required to be performed on cubes and cylinders with different mixed design ratios in the laboratory [16,17].

In the last few years, many mineral admixtures such as rice husk ash [18,19], sugarcane bagasse ash [20,21], corn cob ash [22,23], electric arc furnace dust [24,25], rice straw ash [26,27], coal bottom ash [28,29], waste paper sludge [30,31] and metakaolin [18,32] have been utilized as a partial replacement of cement to enhance the performance of manufactured concrete in comparison to the conventional concrete. Further, this method is prone to human error, and one small error can cause a lot of time wastage. To overcome this issue, Machine Learning (ML) models of Artificial Intelligence (AI) shall be considered the best option. In fact, ML has been widely used in several civil engineering applications [33–35]. In recent times, ML has emerged as a powerful tool to predict the output parameter, i.e., compressive strength, of different types of concrete using various algorithms [36–39]. Yaseen et al. [40], conducted a study using an advanced ML model, namely an extreme learning machine (ELM), to forecast the compressive strength of foamed concrete with cement content, foam volume, density and water-to-binder ratio as input parameters. The performance of ELM model was compared with the other algorithms, such as multivariate adaptive regression spline (MARS), M5 tree model, and SVM. The output of the study indicated that ELM exhibited the most precise prediction with the least errors. Ashrafian et al. [41] utilized MARS, along with the water cycle model, to predict the compressive strength of lightweight concrete, and it was observed that the hybrid AI algorithm provides improved prediction. Young et al. [42] carried out a study that involved the application

of ANN, DT and SVM with a significantly large dataset (>10000) obtained from laboratory and industry scale-based concrete mixtures to predict the compressive strength. The study showed models have accurately predicted the compressive strength of laboratory-manufactured concrete than to industry based-concrete mixtures. Apart from compressive strength, studies on the predictions of shear strength of beams and bar length have also been carried out to assist/prior to construction activities [43,44]. Besides these models, a few studies have also used RF [16], Hydrostatic-Seasonal-Time (HST) model [45], Multilayer Perceptron (MLP) [46], Convolutional neural networks (CNN) model [47,48], Gaussian Processes (GP) [49], M5P [50], long short-term memory networks (LSTM) model [51], multiple linear regression (MLR) [52], gene expression programming (GEP) [53] and linear regression [54] to predict compressive strength and other parameters of waste-based concrete along with different input parameters and obtained the adequate outputs [55–57].

1.1. Research significance

Besides the employment of ML models, numerous experimental studies have been conducted by several researchers on the effect of the addition of fly ash on the compressive strength of concrete [58–61]. Only a chunk of studies has been carried out on the prediction of compressive strength of fly-ash-based concrete using the ML models. Researchers have adopted gene expression programming GEP, SVM, ANN, MLR and some other models to forecast the compressive strength of fly-ash concrete and obtained good accuracy with low errors [16,39,62]. However, most of the studies have used very few models using a smaller number of input parameters. Also, the performance of the models had not been checked adequately as the execution of a few assessments had been reported on the prediction of strength parameters for fly-ash-based concrete. In addition, the use of silica content, lime content, iron oxide content and aluminum oxide as input parameters hasn't been reported for predicting the strength of concrete. Considering these shortcomings, the current study aims to predict the compressive strength of fly ash-based concrete through nine different ML models such as Linear Regression (LR), Gradient Boost (XGboost or GB), Random Forest (RF), Decision Tree (DT), Support Vector Machines (SVM) regression, M5P, Gaussian Processes (GP), Multilayer Perceptron (MLP) and Artificial Neural Network (ANN). Twelve input parameters, i.e., replacement percentage, water-cement ratio, cement content, fine aggregate content, coarse aggregate content, water content, silica content, lime content, iron oxide content, aluminium oxide content, the specific gravity of fly ash and the number of curing days, have been taken into investigations. The comparison of the aforementioned models has been carried out on the basis of descriptive statistics, least errors, coefficient of correlation (R^2), Taylor's diagram, feature importance and parametric analysis. Through the employment of the approach considered in the current study, suitable insights regarding the usage of more sophisticated ML models as well as significant research gaps, have been enlisted in the article.

2. Machine learning models implied in the present study

2.1. Linear regression (LR)

LR is the most common predictive model of supervised learning. It is used to identify the relationship among the variables [63,64]. It sets a linear relationship between the input (x-axis)

and output (y-axis). It distinguishes the influence of the independent input variables from the dependent variables [65]. This ML algorithm fits a straight line around the mapped numeric inputs and outputs. The expression for LR is as follows:

$$\hat{y} = f(x_i, \beta_i) + e_i \quad (1)$$

Where, $\hat{y}$ = dependent variable, x_i = independent variable, β_i = coefficients, e_i= errors in regression.

2.2. Decision tree (DT)

DT model is the most popular and easy-to-read supervised ML model. Its path always begins from the root node [39,66]. DT has two types of nodes: the branch node represents the decision, and the leaf node shows the outcome [67]. Any Boolean function can be represented on discrete attributes. It uses multiple algorithms that split one node into two to more sub-nodes. In DTs, for the prediction of outcome, the analysis starts from the root node of the tree. This process continues and carries on comparing the internal nodes until the leaf node reached to the predicted outcome [68]. The expression for DT is given below:

$$Gain(S, A) = E(S) \sum_v \frac{|S_v|}{|S|} E|S_v| \quad (2)$$

Where, $Gain(S, A)$ = entropy gain of samples 'S' on attribute A, $E(S)$ = entropy of the entire sample 'S, S_v = sample belonging to subset 'v', $E|S_v|$ = entropy of sample belonging to subset 'v'.

2.3. Support vector machine (SVM)

An SVM is a supervised learning model that is mainly used to solve classification problems in ML. The algorithm takes the data, sorts it into one or more groups depending upon the input, and represents it in different classes in the hyperplane of multidimensional space. This hyperplane boundary segregates n-dimensional space into subclasses so that it can easily put the new data point in their category in the future. The main aim of the hyperplane is to "maximizes the margin" between classes. An SVM can be linear or nonlinear [69,70]. The SVM algorithm has a technique which is called the "kernel trick". This kernel function converts non-separable problems to separable problems. It simply does some extremely complex data transformations and then finds out the process to separate the data based on the labels or outputs defined by the user [71].

The expression for SVM is given below:

$$y = f(x) = w.x + b = 0 \quad (3)$$

Where, w = a vector normal to hyperplane, b = an offset.

2.4. Gradient boost (GB)

GB is an effective boosting algorithm used in many applications [16,72,73]. In the prediction models, each prediction corrects its predecessor's error. It works on the principle that many weak

learners, such as a decision or shallow trees, can work together to form a precise and accurate predictor. A weak learner model is a model that does slightly better than random predictions. DTs are used as the weak learner in GB. It provides a prediction model in the form of an ensemble of weak DT prediction models. The expression for GB is given below:

$$G_x\,(x) = G_n - 1(x) + h_n(x) \tag{4}$$

Where, $G_x(x)$ is the Gradient boost regression model, $h_n(x)$ is the weak learner.

2.5. Random forest (RF)

RF is a supervised model that can be used for both regression and classification problems. It is a learning method that consists of many DTs. In classification problems, the prediction with the most votes is considered the outcome. Moreover, in regression problems, the outcome is taken as the average of all the predictions [38,74–76]. It is versatile to be applied to large-scale problems. The expression for regression problems is as follows:

$$MSE = \frac{1}{V}\sum_{i=1}^{V}(f_i - p_i)^2 \tag{5}$$

Where, MSE is the mean squared error, V = number of data points, f_i = value returned by the model, p_i = actual value for data point i.

2.6. Artificial neural network (ANN)

Artificial neural networks, also known as neural networks, are made up of artificial neurons that are designed in a way to work as a human brain. It is an information-processing paradigm that is inspired by the human brain. There are three layers: the input layer, the hidden layer (one or more) and the output layer [77–79]. Every neuron is connected to another neuron and transfers the data from one layer to another neuron of the next layers. In this way, the data reaches the last layer that is called the output layer of the neural network and generates the output. The expression for this model is:

$$w_x^* = w_x - a\frac{\partial(error)}{\partial(w_x)} \tag{6}$$

Where, w_x^* = new weight, w_x = old weight, a = learning rate, $\frac{\partial(error)}{\partial(w_x)}$ = derivative of the error with respect to weight.

In addition, Multilayer Perceptron (MLP) has also been used in the current study to predict the compressive strength of fly-ash-based concrete. It is a type of artificial neural network that consists of multiple layers of interconnected nodes and is widely used for applications including pattern recognition, classification, and regression [80,81]. The weights and biases in an MLP can be learned through training, where the network is presented with input-output pairs, and the parameters are updated to minimize the error between the actual and predicted outputs. This process is typically done using optimization algorithms such as gradient descent or back propagation. The expression of a single artificial neuron in an MLP can be represented as:

$$\gamma = \vartheta(b + \sum(w_i x_i)) \tag{7}$$

Where, γ is the output of the neuron, ϑ is the non-linear activation function, b is the bias involved, w_i indicates the vector of the weights and x_i is the input of the vectors.

2.7. M5P

The M5P model, also known as the M5 Model Tree, is a decision tree-based model that uses linear regression at the leaves. The model tree consists of a series of decision nodes and linear regression models at the leaves, where each decision node splits the data based on a test condition, and the linear regression models at the leaves are used to make predictions for the observations that fall into that leaf [50,82]. The expression of an M5P model can be represented as follows:

$$SDR = sd(\mathrm{H}) - \sum \left| \frac{H_i}{H} \right| \times sd(\mathrm{H}_i), \tag{8}$$

$$\mathrm{sd(H)} = \sqrt{\sum_1^N \frac{((H_i - \overline{H}))^2}{N-1}}, \tag{9}$$

$$\overline{H} = \sum_i^N \frac{H_i}{N}, \tag{10}$$

Whereas *SDR* is the standard deviation reduction factor, $sd(\mathrm{H})$ is the standard deviation of H, H is the dataset that stretches the node, H_i is the set that established from a divided node.

2.8. Gaussian processes (GP)

Gaussian Processes (GP) are a type of probabilistic model used for regression and classification tasks in ML [49,50,83] and provide a flexible and non-parametric approach to complex modelling relationships between inputs and outputs. GP defines a distribution over functions, where each function is considered a random variable. The covariance function can be chosen to reflect prior knowledge about the behaviour of the underlying function, such as smoothness or periodicity. The expression can be defined as:

$$h(\mathrm{x}) \sim \mathrm{GP}(\mathrm{m}(.), \mathrm{k}(.,.)) \tag{11}$$

Whereas $h(\mathrm{x})$ is the random variable representing the function value at the input *X*, $\mathrm{m}(.)$ is the mean function, providing the expected value of the function for a given input X, $\mathrm{k}(.,.)$ is the covariance function, describing the relationships between the function values for different inputs $(.,.)$, and GP is the GP distribution over functions.

3. Methodology

The methodology considered during the execution of the current work has been presented in this section. Fig. 1 illustrates the general processes involved during the development of the ML models.

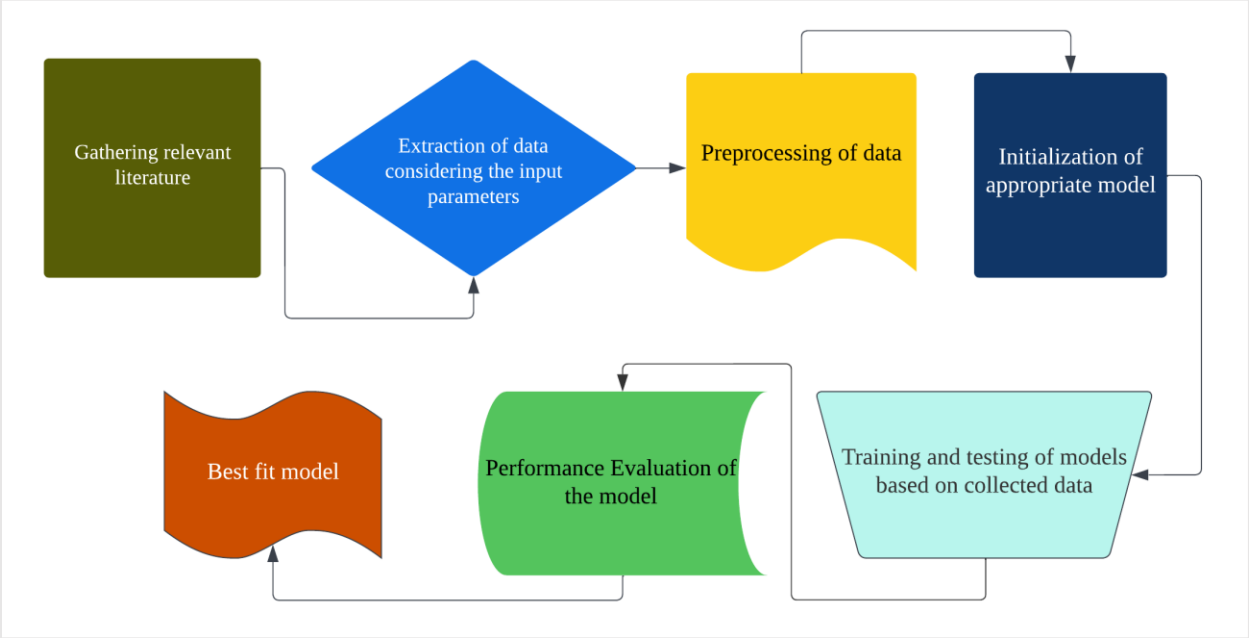

Fig. 1. Approach adopted in the existing study while developing the ML models.

3.1. Data collection

A total of 455 data points have been collected in terms of replacement percentage, water-cement ratio, cement content, fine aggregate content, coarse aggregate content, water content, silica content, lime content, iron oxide, aluminium oxide, the specific gravity of fly ash and number of curing days from the relevant literature on the use of fly ash in concrete [58,84–109]. Out of 455 data points, 364 (80%) and 91 (20%) data points were used for the training and testing of the ML models, respectively. During the data collection process, a criterion was defined where studies with most input parameters were considered for analysis purposes. For example, the articles where the information regarding the input parameters, such as water-cement ratio, the content of cement, coarse aggregate or fine aggregate, was missing were exempted from the dataset. While extracting the data, the previous studies involving the replacement of cement with fly ash to manufacture concrete were carefully examined and considered.

3.2. Data pre-processing

The pre-processing of the collected data has been performed using imputation. Additionally, the scaling of the data set in terms of 0 and 1 for mean and standard deviation has been assigned, respectively.

3.3. Initializing, training and testing and running the models

During the initialization of the models, default parameters were assigned to the LR, DT, M5P , RF and SVM models, whereas, in the case of XGBoost , "reg:squared error." is assigned as the objective. Multistart optimization strategy is used to estimate the model parameters to train GP. In the case of the ANN and MLP model, each layer has been defined differently. One input, one hidden and one output layer were assigned to six, three and one unit. Each model has been trained on the processing and respective data of compressive strength. Followed by the testing, the models were tested for errors, co-relationship between the data set, Taylor's diagram and feature importance analysis. After the testing and training, the whole data set was used to predict the output.

3.4. Tools utilized

In the current study, the tools such as Jupyter notebook (version 5.0.0), Pyscripter (version 2.0), Origin Lab (versions 9 and 12) and Microsoft Excel (version 2016) have been used for writing the codes, analysis and plotting the graphs.

4. Result and discussion

4.1. Scatter plots

Scatter plots are used to show the values for two different numeric variables using dots. These plots are used to analyze the relationship between the different variable inputs and make use of Cartesian coordinates to represent the values of the variables in a data set [110,111]. The scatter plots of the current study are shown in Fig. 2.

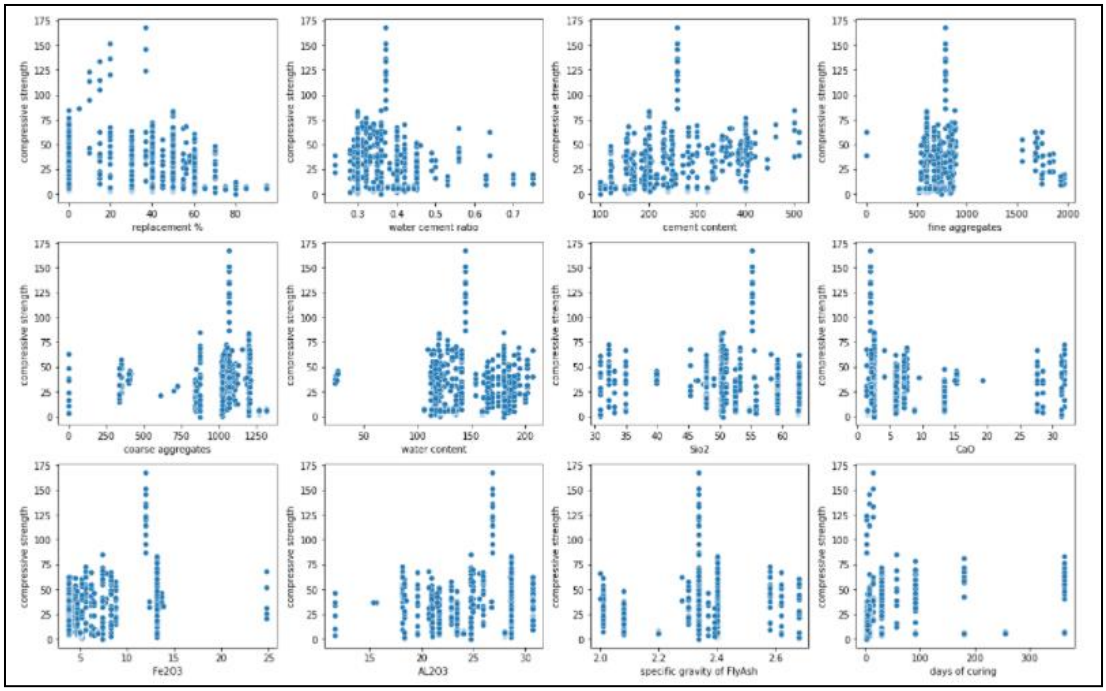

Fig. 2. Scatter plots of Input parameters vs Compressive strength.

Based on Fig. 2, it can be inferred that the input parameters are directly associated with the compressive strength. Each model works in different ways, causing a difference in the output. The linear fit line of data points shows the strong relationship between one input parameter corresponding to the compressive strength. Whereas in some of the plots, a moderate linear relationship has been observed. The involvement of a new variable significantly correlated with a variable in the prior step equation will not produce a better prediction equation because the new attribute is coded data of a parameter already in the analysis. The results of the current study are in line with the trend noticed in the previous studies [112–114].

4.2. Descriptive statistic

Descriptive statistics are a set of tools used to summarize and describe the characteristics of a dataset as it provides a way to organize and present data in an informative way [115,116]. It summarizes large and complex datasets by reducing them to a few key numbers or measures. Descriptive statistics enables the identification of patterns and trends in data, such as the mean, median, and mode, that can indicate underlying issues or opportunities. It also aids in detecting outliers, i.e., values that fall outside the range of the typical data. The descriptive statistics of the data used to forecast CS is presented in Table 1.

Table 1
Descriptive statistics of the input and output parameters [58,84–109]

Variable	Statistics					
	Min	**Max**	**Avg**	**StDev**	**Sk**	**Kt**
Water-cement ratio	0.24	0.88	0.39	0.11	2.02	4.91
Cement content	93	510	236.20	92.01	0.74	-0.39
Fine aggregate	0	1970	791.67	295.43	2.01	4.68
Coarse aggregate	0	1990	1053.12	303.63	-0.90	2.21
Water content	22.7	270	154.05	40.39	0.48	0.73
SiO_2	30.9	68.4	53.59	8.92	-1.08	0.57
CaO	1.21	31.9	7.13	8.60	1.91	2.50
Fe_2O_3	3.48	24.83	6.85	3.36	2.28	7.24
Al_2O_3	11.6	30.7	24.86	3.81	-0.70	0.39
Specific gravity	2	2.68	2.35	0.18	-0.49	-0.25
Curing days	1	365	72.86	105.24	1.84	2.28
Replacement Percentage	0	95	47.69	17.50	-0.23	-0.32
Compressive strength	0	167.75	31.67	23.06	1.38	4.13

Note: **Min**-Minimum; **Max**-Maximum; **Avg**- Average; **StDev**-Standard Deviation; **Sk**-Skewness; **Kt**-Kurtosis

4.3. Correlation matrix

A correlation matrix is a table showing the correlation coefficients between multiple variables. It is a useful tool for understanding the relationships between different variables in a dataset, identifying multi-linearity and outliers, and can aid in identifying dependent and independent variables that can support further analysis and modelling. A correlation coefficient of 1 indicates a perfect positive correlation, a coefficient of -1 indicates a perfect negative correlation, and a coefficient of 0 indicates no correlation [115,117,118]. In the context of the current study, the concrete variables are dependent on each other. Therefore, the coefficient of correlation of all variables has been extracted and shown in Table 2 and Fig. 3.

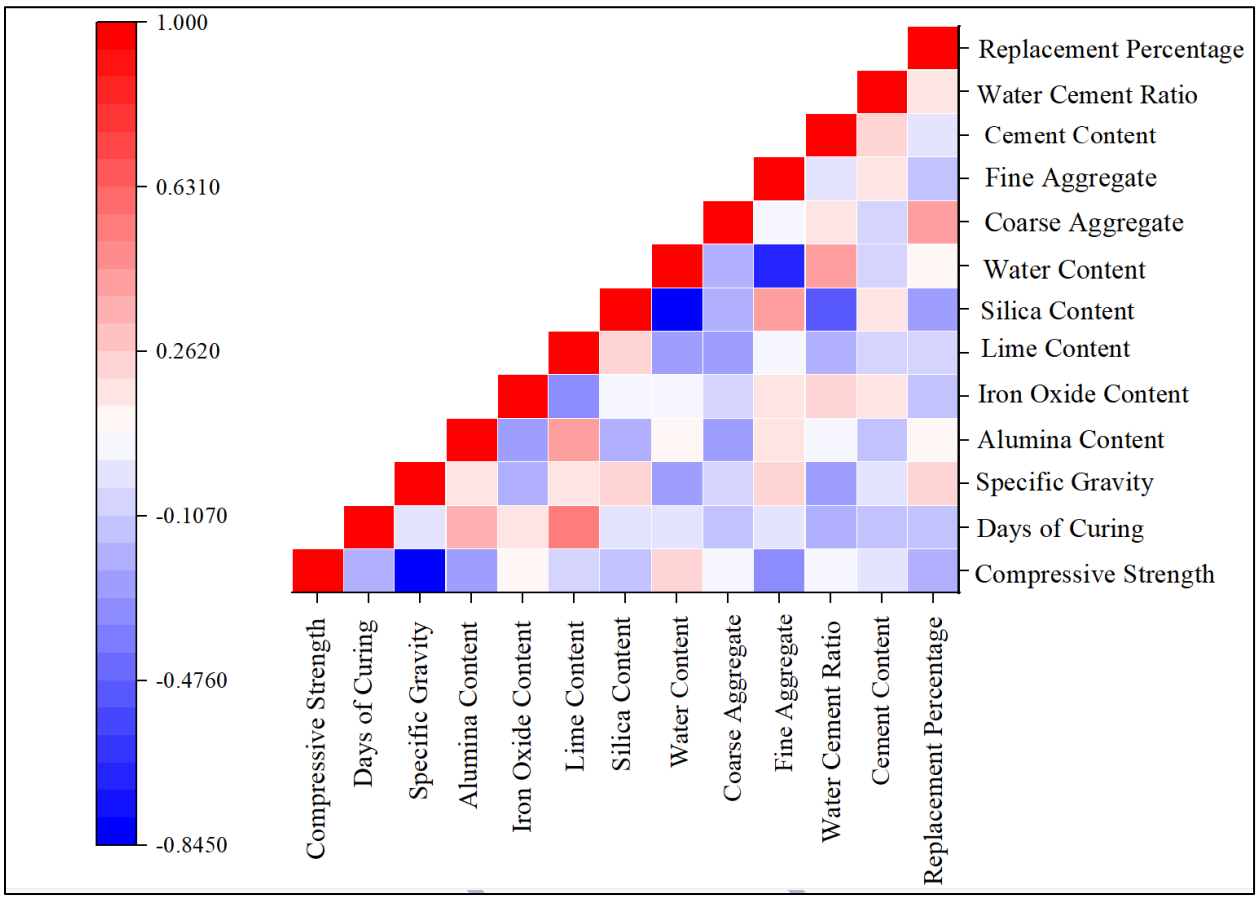

Fig. 3. Correlation matrix in the form of Heat map for the variables considered in the current study

Fig. 3. shows the correlation matrix of the parameters undertaken in the study. The greater difference in the positive and negative values of the correlation coefficient between the input parameters could be responsible for the poor efficiency and complexity in evaluating the effect of these parameters on the response [119].

Table 2
Correlation Matrix of input and output parameters.

Variables		Input Parameter												Output Parameter
		RP	**W-C ratio**	**CC**	**Fi-ag**	**Co-ag**	**W-C ratio**	**SiO_2**	**CaO**	**Fe_2O_3**	**AL_2O_3**	**SG**	**DOC**	**CS**
Input Parameter	**RP**	1.00	-	-	-	-	-	-	-	-	-	-	-	-
	W-C ratio	-0.22	1.00	-	-	-	-	-	-	-	-	-	-	-
	CC	-0.84	0.01	1.00	-	-	-	-	-	-	-	-	-	-
	Fi-ag	-0.25	0.38	0.15	1.00	-	-	-	-	-	-	-	-	-
	Co-ag	0.09	0.16	-0.18	-0.23	1.00						-	-	-
	W-C ratio	-0.10	0.55	0.16	0.43	-0.32	1.00	-	-	-	-	-	-	-
	SiO_2	-0.14	0.01	0.23	-0.22	0.06	0.24	1.00	-	-	-	-	-	-
	CaO	0.24	0.00	-0.28	0.11	0.05	-0.23	-0.83	1.00	-	-	-	-	-
	Fe_2O_3	0.03	-0.13	-0.10	-0.29	-0.10	-0.23	-0.22	-0.17	1.00	-	-	-	-
	AL_2O_3	-0.31	-0.01	0.21	0.17	0.19	0.02	0.45	-0.70	0.03	1.00	-	-	-
	SG	0.02	-0.21	-0.25	0.04	0.24	-0.20	-0.54	0.40	0.17	-0.02	1.00	-	-
	DOC	0.01	-0.12	-0.03	-0.16	0.15	-0.06	0.16	-0.10	-0.06	0.14	0.23	1.00	-
Output Parameter	**CS**	-0.22	-0.11	0.23	0.09	-0.14	-0.06	-0.28	0.08	0.39	-0.11	-0.01	0.15	1.00

Note: **RP**- Replacement Percentage; **W-C ratio**- Water Cement Ratio; **CC**- Cement Content; **Fi-ag**- Fine Aggregate; **Co-ag**- Coarse Aggregate; **SG**- Specific Gravity; **DOC**- Day of curing

4.4. Histogram

A histogram is a graphical representation of data that shows the frequency distribution of a set of continuous or discrete data [48,117,120]. It is a powerful tool for understanding the distribution of data and identifying patterns and trends while identifying outliers which can indicate underlying issues or opportunities. Fig 4, Fig. 6 and Fig. 6 shows the normalized values of input and output parameters in the form of histograms. These graphs are significantly important as they can aid in indicating the range of the values for a particular parameter that is required or insufficient.

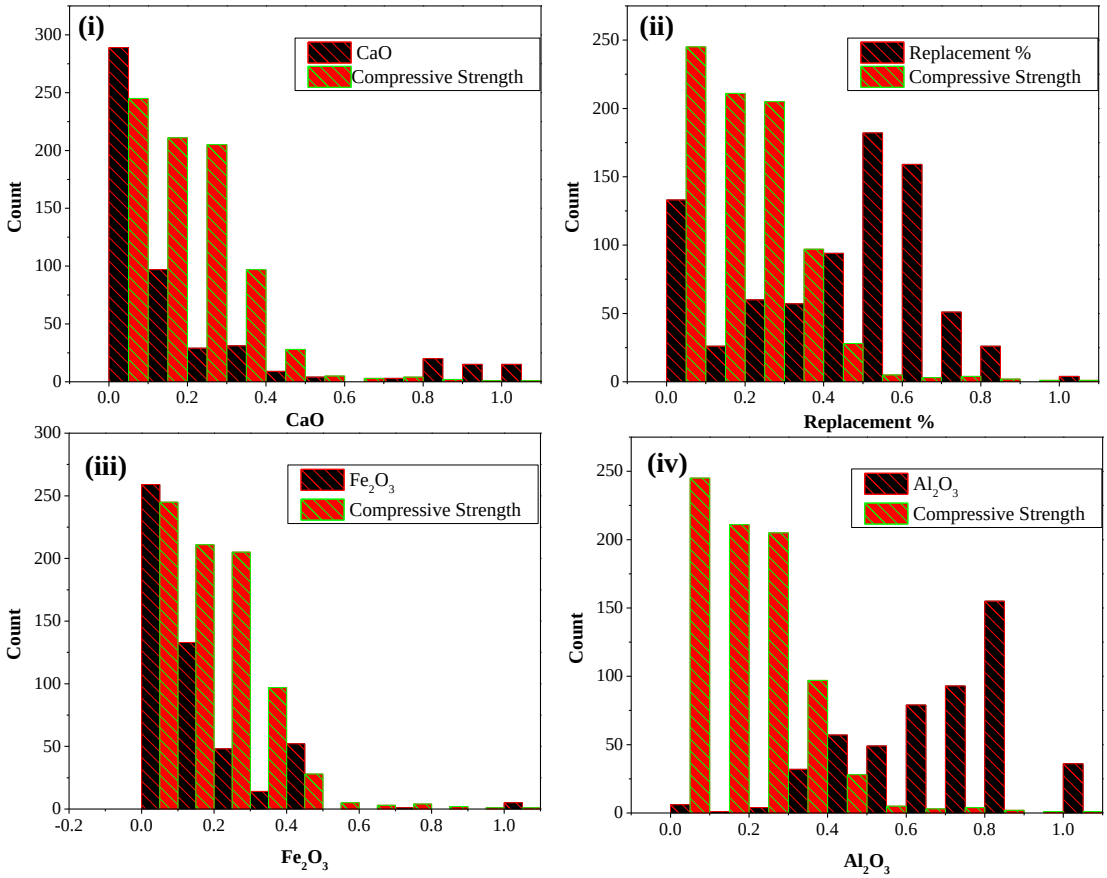

Fig. 4. Combined histogram of input and output variables (i) CaO and CS; (ii) Replacement % and CS; (iii) Fe_2O_3 and CS; and (iv) Al_2O_3 and CS.

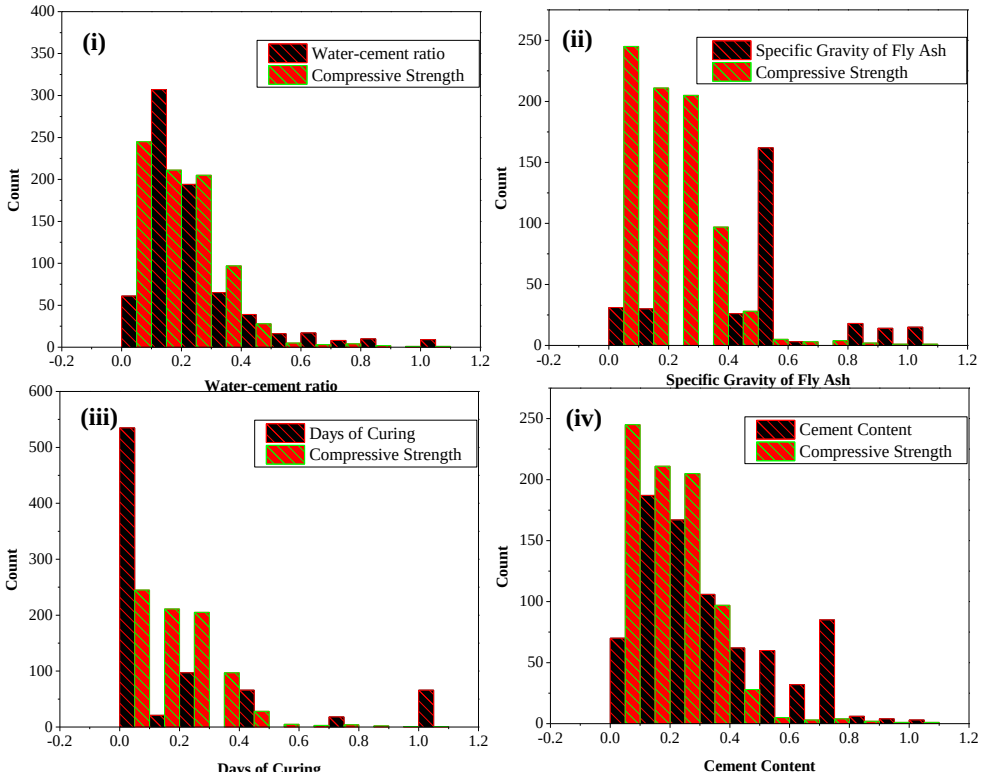

Fig. 5. Combined histogram of input and output variables (i) Water-cement ratio and CS; (ii) Specific gravity and CS; (iii) Days of curing and CS; and (iv) Cement content and CS.

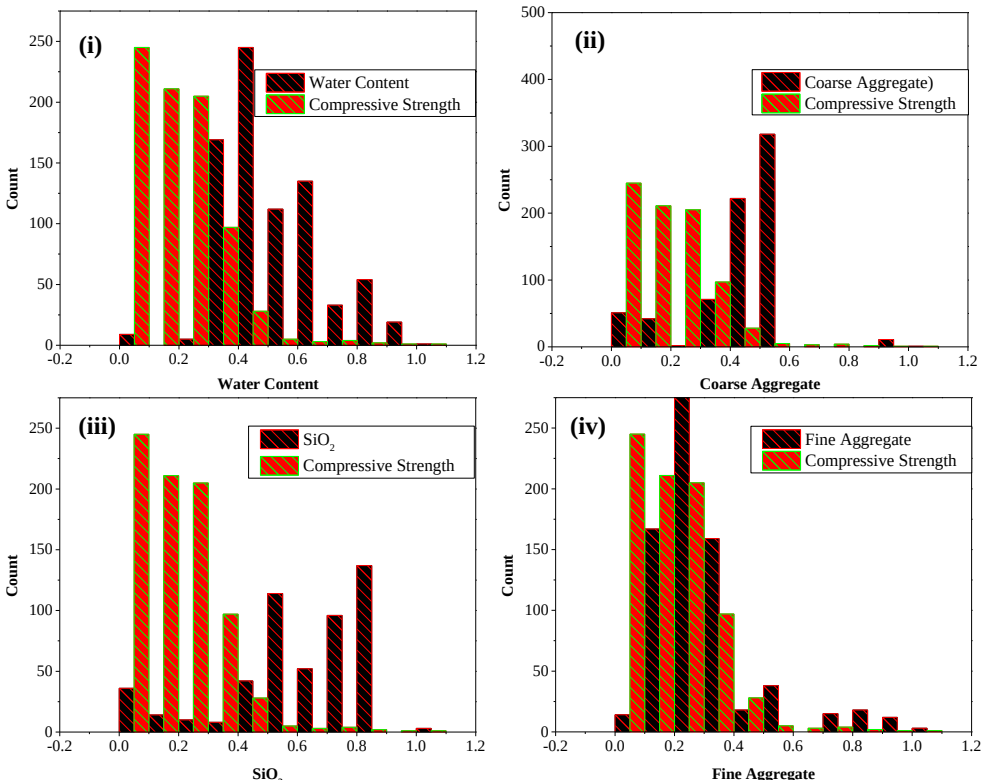

Fig. 6. Combined histogram of input and output variables (i) Water content and CS; (ii) Coarse aggregate and CS; (iii) SiO_2 and CS; and (iv) Fine aggregate and CS.

4.5. Assessment of errors

4.5.1. Mean absolute error

The mean absolute error (MAE) is used for model evaluations. MAE gives the average of the absolute difference between the actual and predicted values in the dataset. It is used to predict the accuracy of the ML model [114,121]. It may not adequately reflect the performance when dealing with large error values. MAE [122] can be calculated as:

$$MAE = \frac{1}{n}\sum_{j=1}^{n}|x_i - \hat{x}_i| \tag{12}$$

Where x_i = predicted value, $\hat{x}_i$ = true value and n = total number of data points

4.5.2. Mean squared error

Mean Squared Error is highly biased for higher values. The MSE defines the closeness of a regression line to a set of points. The lower the value, the better the model. If the value is 0, that means the model is perfect. To calculate MSE [114,122], the following is the formula:

$$MSE = \frac{1}{t}\sum_{i=1}^{t}(x_i - \hat{x}_i)^2 \tag{13}$$

Where, t = the number of samples, x_i = observed value, $\hat{x}_i$ = predicted value.

4.5.3. Root mean squared error

RMSE is better in terms of reflecting performance when dealing with large error values. It is the standard deviation of the errors that occurs when the prediction is made on the given dataset. It is similar to the mean squared error (MSE), Although the root of its value is considered during determining the model's accuracy [57,123]. It can be calculated as

$$RMSE = \sqrt{\frac{1}{t}\sum_{i=1}^{t}(x_i - \hat{x}_i)^2} \tag{14}$$

Fig. 7 shows the values of MAE, MSE, and RMSE found during the analysis.

Fig. 7. indicated that models such as DT, RF XGboost and M5P performed much better than LR, SVM, ANN, MLP and GP in terms of the occurrence of errors. The output of the current study has been found to be comparable to the ones available in the literature [114,123,124].

4.6. Coefficient of correlation (R^2)

The coefficient of correlation is a statistical measure of how close the data are to the fitted regression line. It represents the variation in the dependent variable which is predicted from the independent variable(s) in a regression model. The higher R^2 value illustrates the fitness of the model according to the reference data [123,125]. The relationship between the experimental and predicted compressive strength by each of the ML models considered in the current study is presented in Fig. 8, Fig. 9, Fig. 10, Fig. 11, Fig. 12, Fig. 13, Fig. 14, Fig. 15 and Fig. 16.

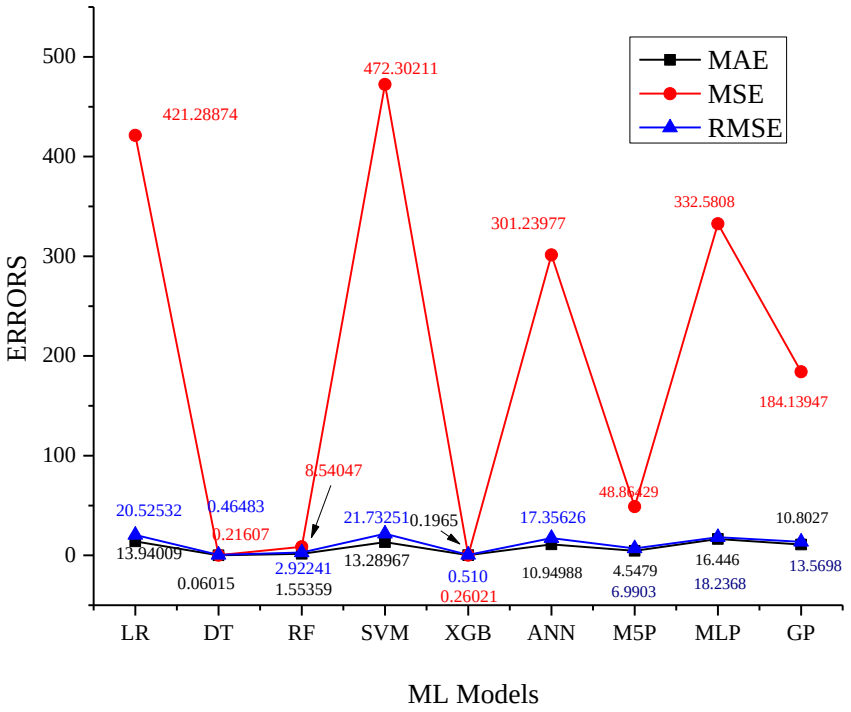

Fig. 7. Values of Errors corresponding to each model.

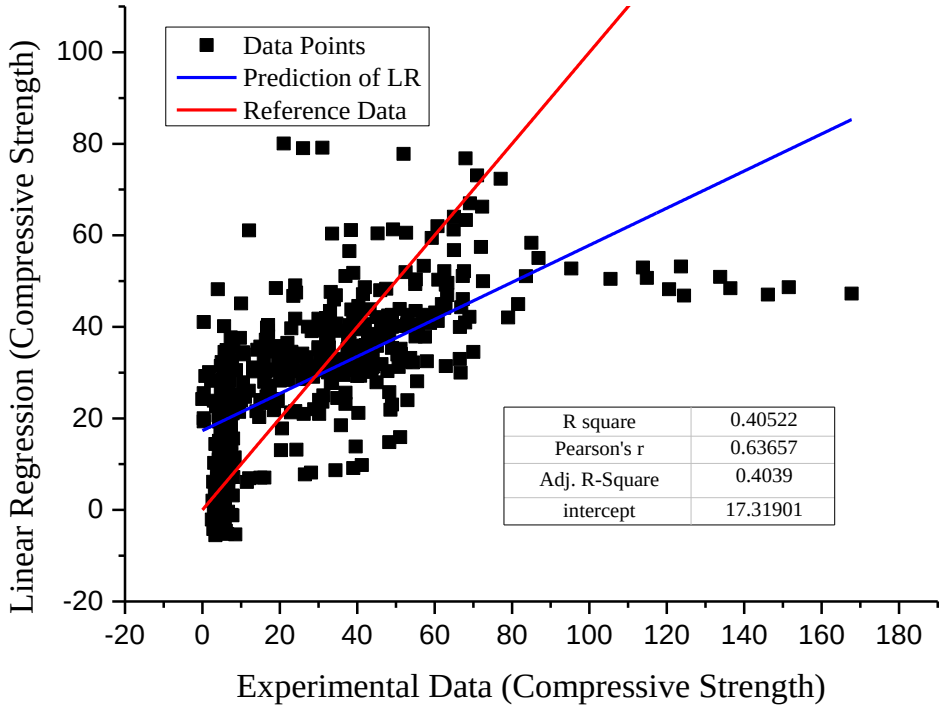

Fig. 8. Correlation ship between the Predicted value of LR vs experimental data.

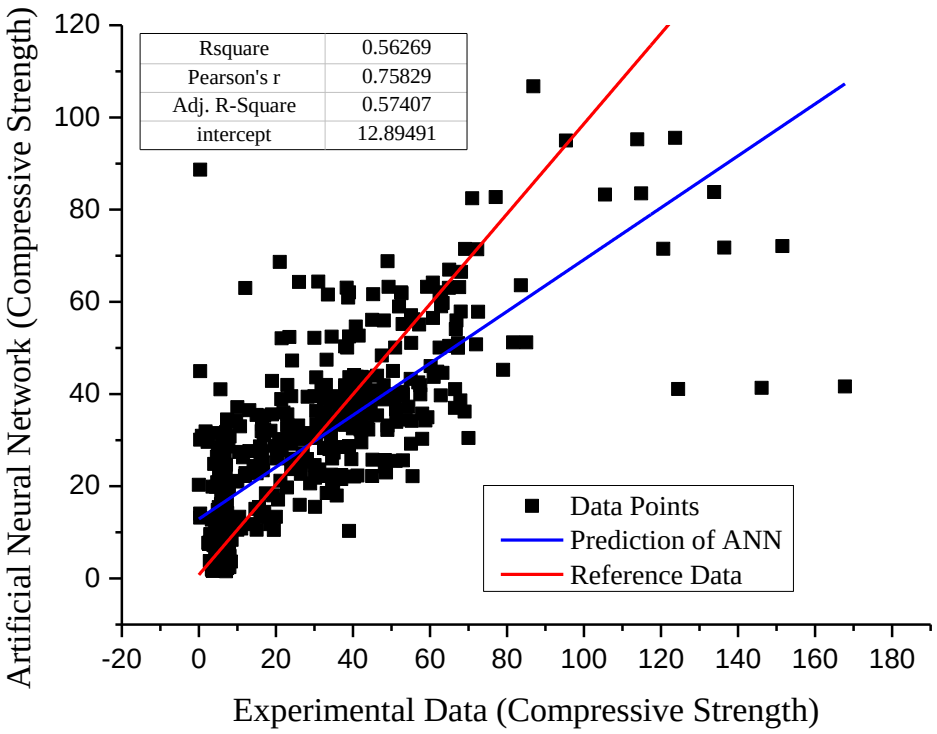

Fig. 9. Correlation ship between the Predicted value of ANN vs experimental data.

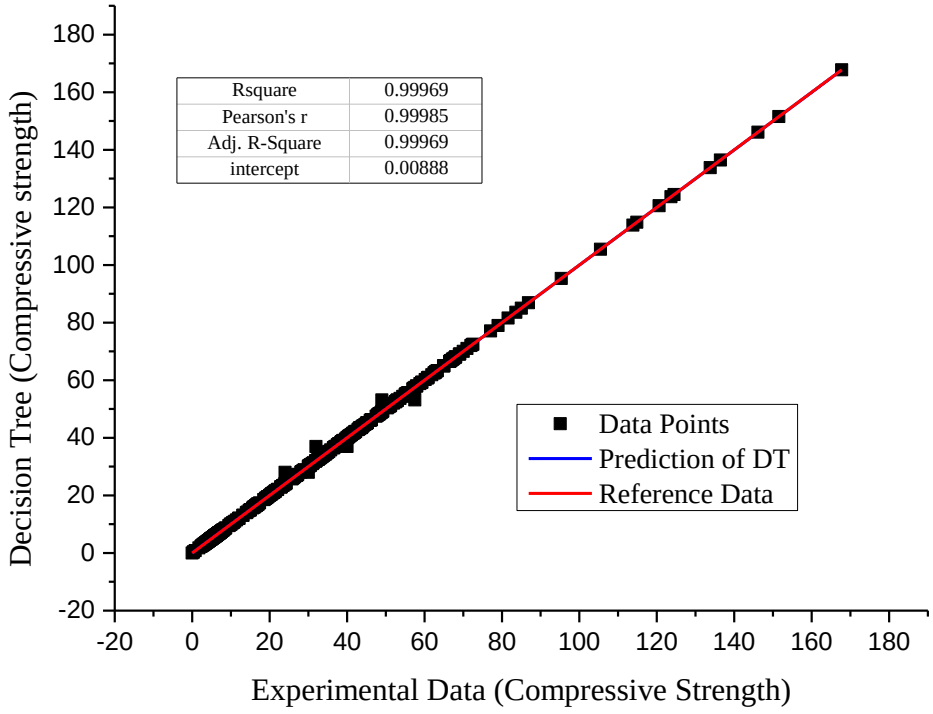

Fig. 10. Correlation-ship between the Predicted values of DT vs experimental data.

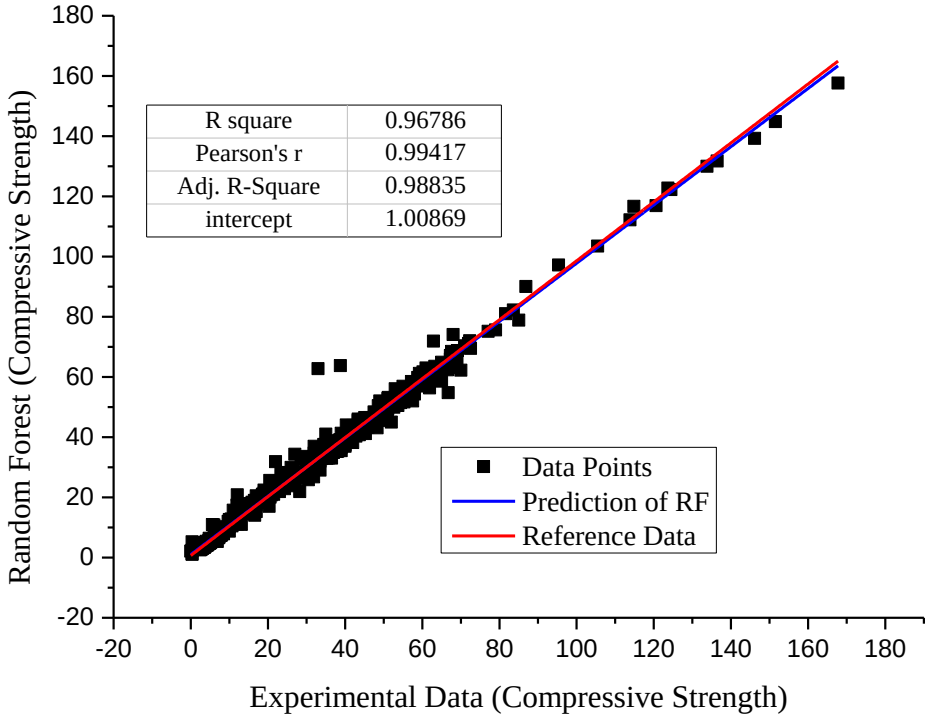

Fig. 11. Correlation ship between the Predicted values of RF vs experimental data.

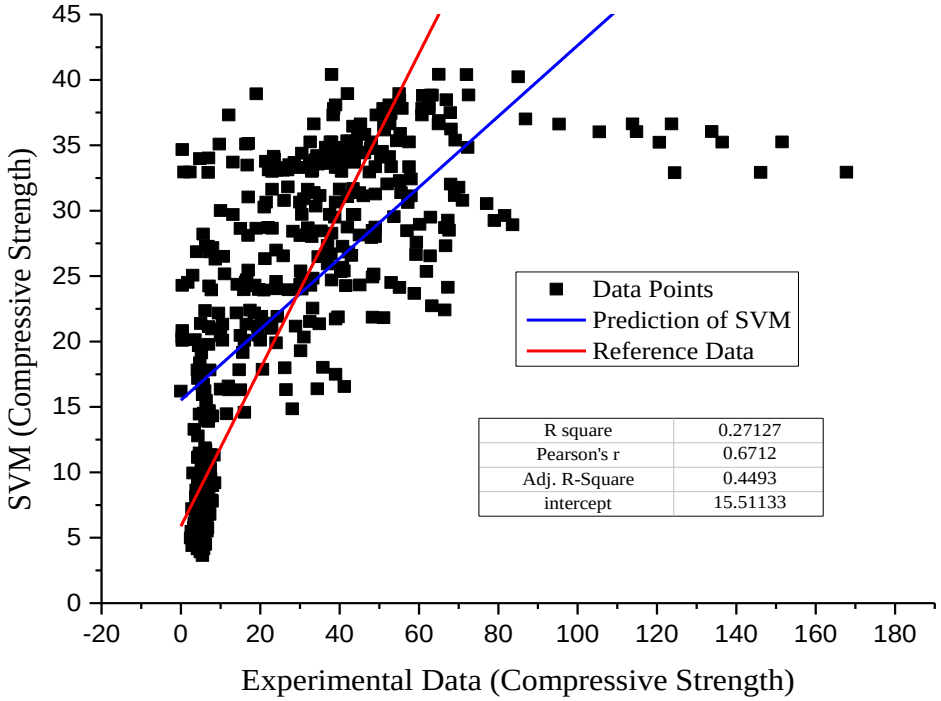

Fig. 12. Correlation ship between the Predicted values of SVM vs experimental data.

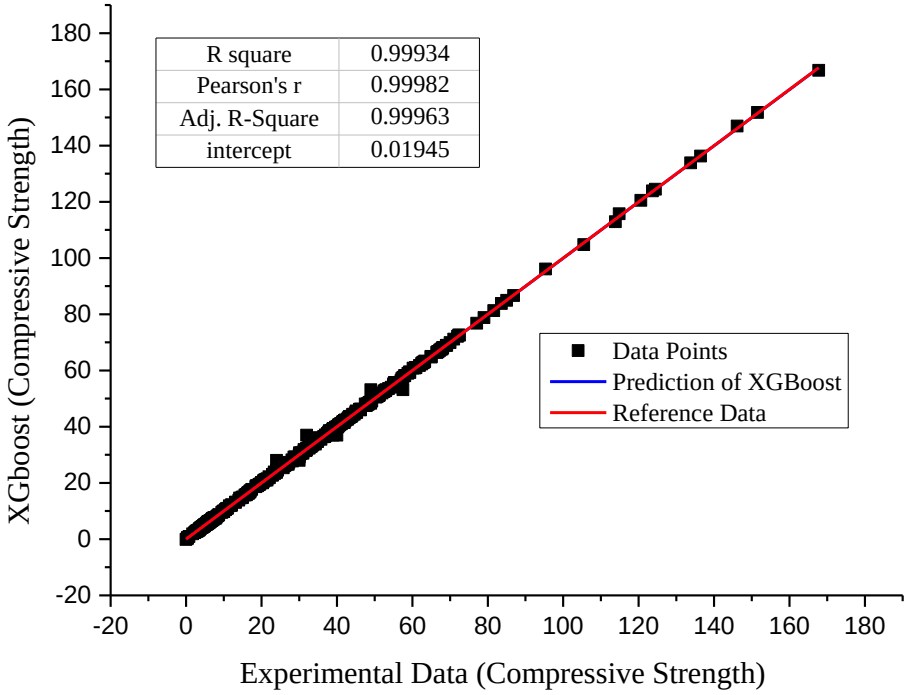

Fig. 13. Correlation ship between the Predicted values of XGboost vs experimental data.

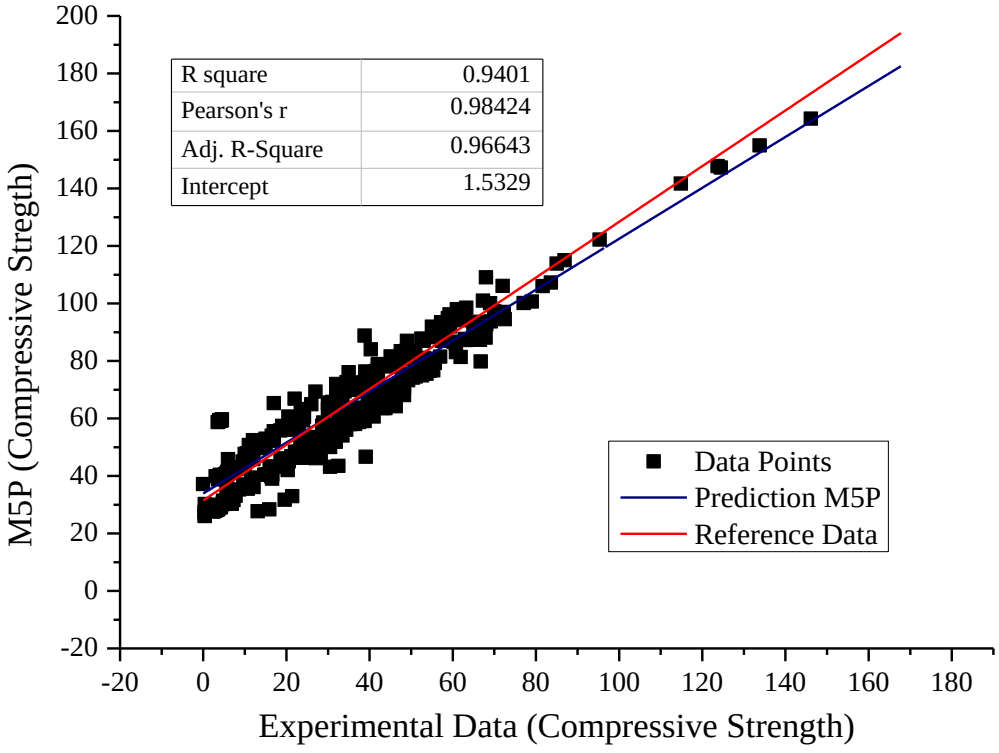

Fig. 14. Correlation ship between the Predicted values of M5P vs experimental data.

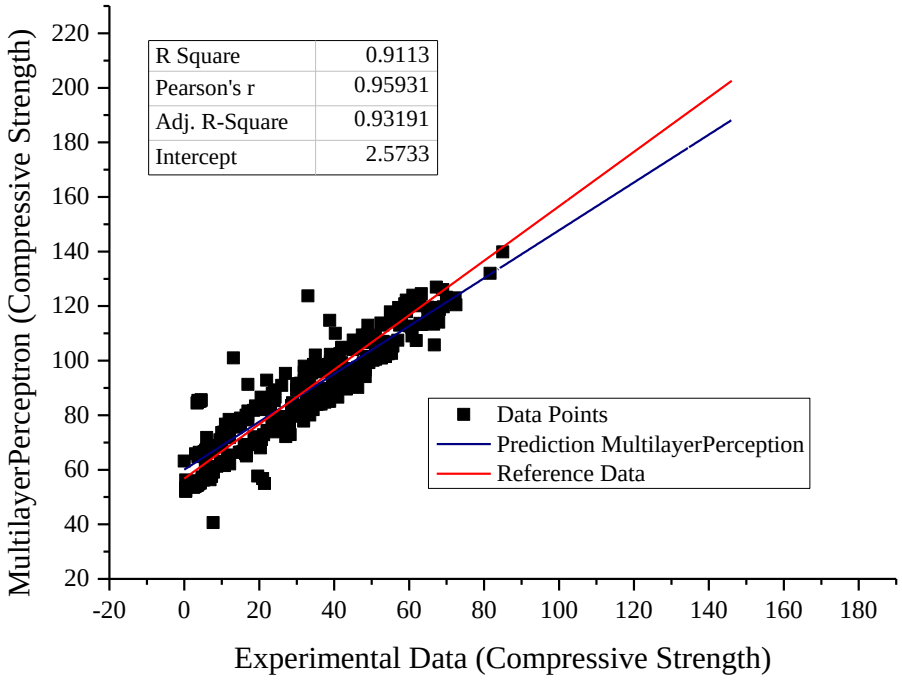

Fig. 15. Correlation ship between the Predicted values of MLP vs experimental data.

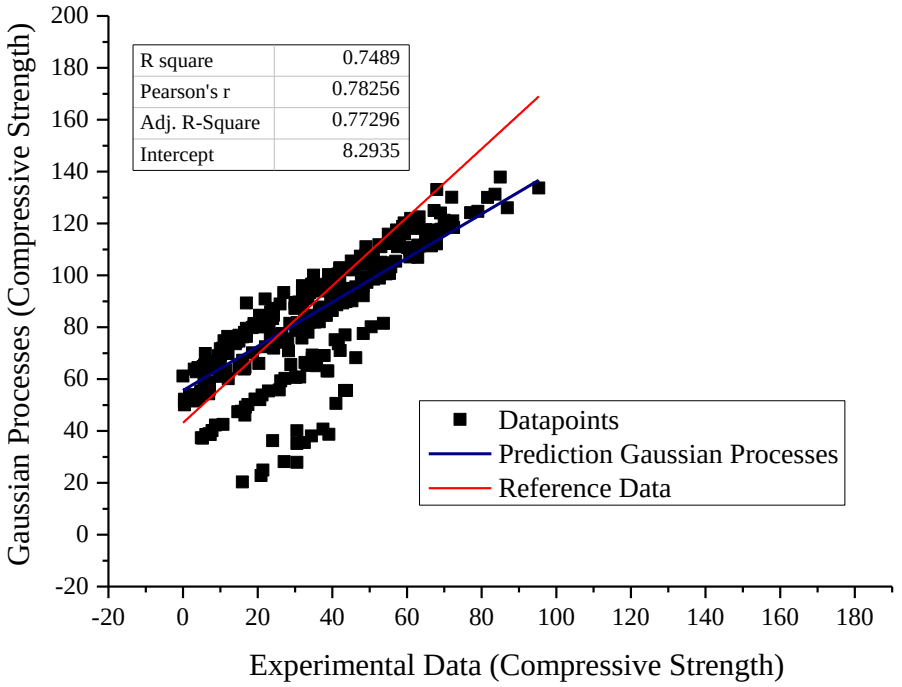

Fig. 16. Correlation ship between the Predicted values of GP vs experimental data.

Based on Fig. 10, Fig. 11, Fig. 13, Fig. 14 and Fig. 15, a strong relationship between the trend line of the experimental and predicted data had been observed. The higher R^2 values of these models confirm their best fitness according to the obtained data. Whereas, in the case of Fig. 8, Fig. 9, Fig. 12 and Fig. 16, the poor relationship between the experimental and forecasted

compressive strength has been noticed. DT, XGboost, RF, MLP, and M5P models showed that the relationship between the test and forecasted values of compressive strength is very close to the linear function, i.e., $y = x$ [114]. Whereas, in the case of LR, SVM, ANN and GP, the diagonal and test data points are more dispersed, indicating that the models do not fit well. Poor performance has been observed by SVM with the least R^2 value as it has a large dispersity of the scatter points and a more significant deviation in coincidence. In the previous studies, the lesser number of input parameters corresponding data set has led to the poor performance of the models. However, when a large number of datasets have been used, models have illustrated a better prediction accuracy [54,79]. In context to the present work, ML models such as DT, XGboost, RF, MLP, and M5P have produced excellent results in predicting the compressive strength of fly ash-based concrete. The results of the current study have been found to be identical to the studies reported in the literature [113,114,123]. Table 3 presents the correlation coefficient of ML models.

Table 3
R-Square value of all models.

Models	LR	DT	RF	SVM	XG	ANN	M5P	MLP	GP
R-Square Value	0.4052	0.9996	0.96786	0.27127	0.99934	0.56269	0.9401	0.9113	0.7489

4.7. Feature importance (FI) or sensitivity analysis (SA)

Feature importance (FI) or sensitivity analysis (SA) depicts the process of the uncertainty in the output of a mathematical model or numerical system that can be allocated to different sources of uncertainty in its inputs [114,126]. The FI analysis of various ML models of the current study is presented in Fig. 17.

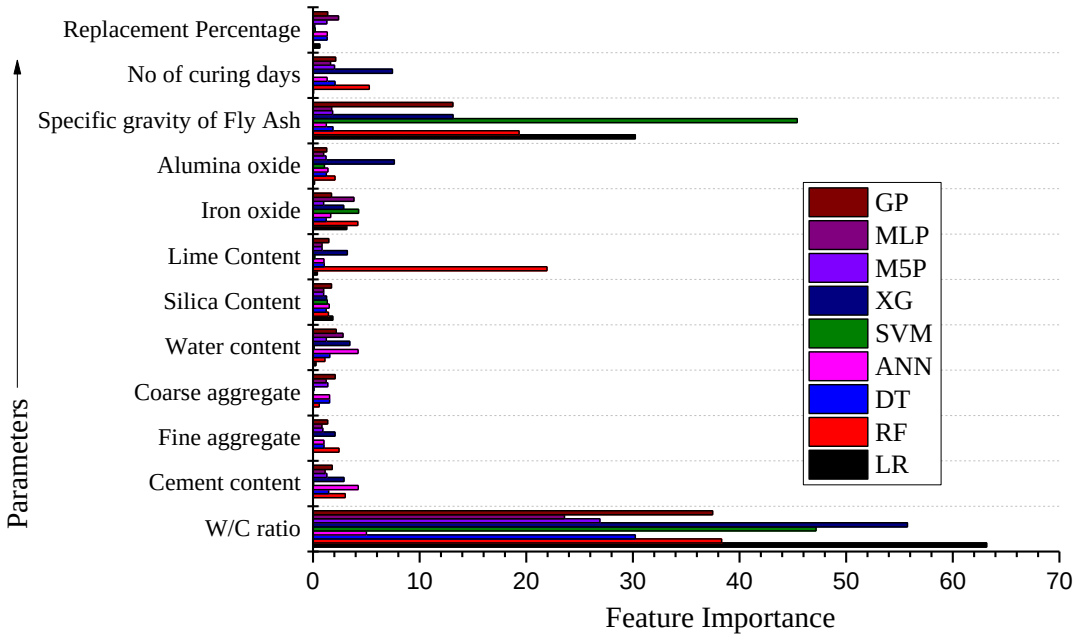

Fig. 17. Feature Importance analysis of ML models.

Based on Fig. 17, it has been noticed that most of the models have considered the specific gravity of fly ash and water-cement ratio as the two most important parameters in determining the compressive strength of fly ash-based concrete. As found in the analysis, input parameters such as replacement percentage, number of curing days, alumina oxide, iron oxide, silica content, water content, coarse aggregate, fine aggregate and cement content have a lesser effect on the compressive strength of fly-ash based concrete. In general, the selection of the most effective input parameter that is directly linked to the output attribute is carried out by the model. In most of the previous studies, input parameters such as water-cement ratio, cement content, replacement levels, and the number of curing days have been selected as the most important parameters which directly affect the compressive strength of the concrete [115,117,127]. In the same line of the previous studies, in the current study, most of the models have preferred the water-cement ratio and specific gravity of fly-ash over other parameters [75,76,114,123].

4.8. Taylor's diagram

Taylor diagram is a visual representation of the degree to which an observed pattern (or combination of observed patterns) matches the reference data. The degree to which two patterns are similar can be measured by comparing their correlation, the centred RMSE difference, and the amplitude of the changes in each pattern (highlighted by their standard deviations) [128]. These diagrams are especially helpful for examining several features of complex models or gauging the relative skill of many distinct models. In the current context, the standard deviation of the experimental data is 26.64 MPa. Fig. 18 represents Taylor's diagram of all the models considered in the current study.

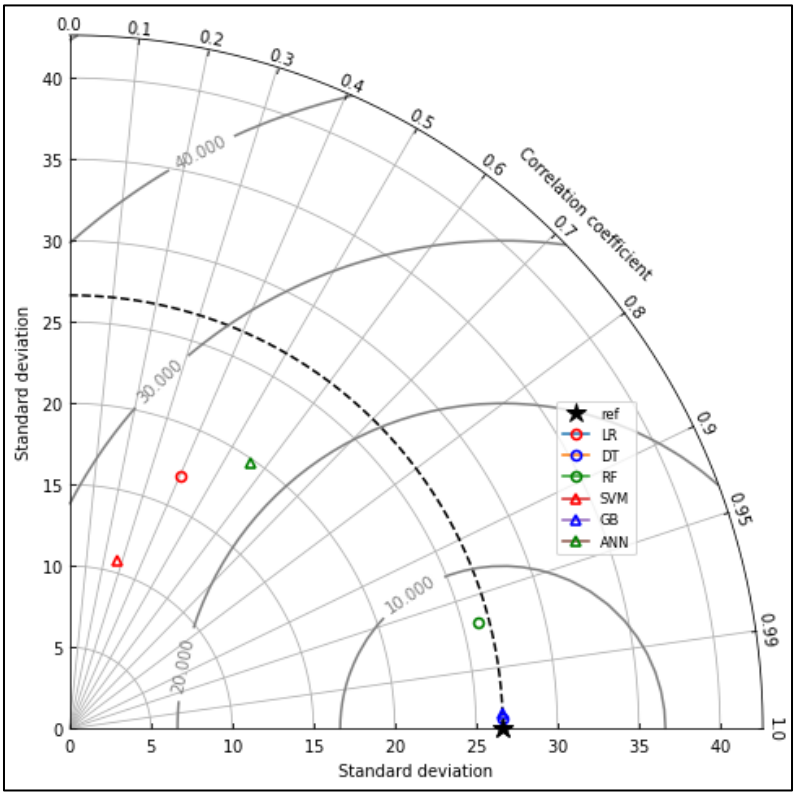

Fig. 18. Taylor's diagram illustrating the performance of the ML models to predict CS.

As observed from Fig. 18, DT and GB models have performed very well and are closer to the reference data as compared to the other models (LR, ANN, SVM and RF). The more excellent correlation value and least RMSE are the two important keys for any model to get a better representation in Taylor's diagram. The output of ML models shown in Fig. 18 is similar to the previous studies [129–131].

5. Conclusions

The current study proposed to predict the compressive strength of fly-ash-based concrete through the utilization of nine different ML algorithms (LR, GB, RF, DT, SVM, M5P, GP, MLP, ANN). In which 12 input parameters (replacement percentage, water-cement ratio, cement content, fine aggregate content, coarse aggregate content, water content, silica content, lime content, iron oxide, aluminium oxide, specific gravity of fly ash and the number of curing days) and 1 output parameter (compressive strength), making an assembly of overall 455 data points, were considered throughout the execution of the study.

It has been observed that the DT and GB models have achieved minor errors and have shown the accuracy of the regressors as compared to other ML models. However, RF and M5P followed the DT and GB models in terms of minor errors and prediction accuracy. The comparison of the output based on the co-relationship between the forecasted and reference data represented that DT and GB have a higher R^2 value (0.99) than the remaining models, such as RF (0.96), M5P (0.94), MLP (0.91), GP (0.74), ANN (0.56), LR (0.40) and SVM (0.27). The representation of the statistical relationship between the experimental and observed data in Taylor's diagram also highlights the optimized performance of DT and GB. The scatter plots illustrated that the input and output parameters defined in the current study have a strong relationship. In addition, FI analysis depicted the parameters that should be considered carefully during the designing and prediction process. It showed that mainly two crucial factors, i.e., the specific gravity of fly ash and water-cement ratio within the mix, have significantly influenced the prediction of compressive strength. However, other input attributes parameters were observed to cause a lesser impact on the compressive strength of the fly ash-based concrete.

The current study provides a better understanding to the researchers and engineers during the decision-making process to choose input parameters and ML models in order to forecast the output parameter, such as compressive strength, with the least errors. The algorithms proposed can be employed on-site for practical application by only providing the values of the quantities of components to be used. However, it should also be taken care that the feed value should be in the same format used in the dataset so that it may compute and estimate the to-be-achieved strength. Further studies can be focused on evaluating any other output parameters out of mechanical and durability attributes of concrete having distinct types of mineral admixtures, for example, sugarcane bagasse ash and metakaolin, along with hybrid and advanced ML models. Apart from comparing the performance of two or more models, a study can also be executed on rectifying/improving the working operation of a poor model to attain optimal results. Although this study accomplishes a positive/negative influence of input parameters of the model on the concrete compressive strength based on the feature importance analysis, future research is still

required to develop a simplified, intelligent analytical model based on more extensive parametric studies.

Acknowledgement

The authors acknowledge the efforts made by their colleagues to improve the quality of the manuscript.

Funding

This research received no specific grant from any funding agency in the public, commercial, or not-for-profit sectors

Conflict of Interest

The authors declare that they have no conflict of interest.

Data availability statement

The data that support the findings of this study are available from the corresponding author, [M Patel], upon reasonable request.

Authors contribution statement

SW: Conceptualization; SW, AB: Data curation; SW, AB: Formal analysis; SW, AB, RS: Investigation; SW, AB, RS: Methodology; MP: Project administration; AB, MP: Resources; SW, AB: Software; RS, MP: Supervision; AB, RS, MP: Validation; RS, MP: Visualization; SW, RS: Writing – original draft; RS, MP: Writing – review & editing.

References

[1] Schwab K. The Fourth Industrial Revolution: what it means, how to respond. World Econ Fourm 2016.

[2] Khan R, Vyas H. a Study of Impact of Brick Industries on Environment and Human Health in Ujjain City (India). J Environ Res Dev 2008;2:421–5.

[3] Pearson TH, Rosenberg R. A Comparitive Study of the Effects of the Marine Environment of Wastes from Cellulose Industries in Scotland and Sweden 2008;5:77–9.

[4] Bildirici ME. Cement production , environmental pollution , and economic growth : evidence from China and USA. Clean Technol Environ Policy 2019. https://doi.org/10.1007/s10098-019-01667-3.

[5] Benhelal E, Zahedi G, Shamsaei E, Bahadori A. Global strategies and potentials to curb CO2 emissions in cement industry. J Clean Prod 2013;51:142–61. https://doi.org/10.1016/j.jclepro.2012.10.049.

[6] MacLaren DC, White MA. Cement: Its chemistry and properties. J Chem Educ 2003;80:623–35. https://doi.org/10.1021/ed080p623.

[7] Hanifa M, Agarwal R, Sharma U, Thapliyal PC, Singh LP. A review on CO2 capture and sequestration in the construction industry: Emerging approaches and commercialised technologies. J CO2 Util 2023;67:102292. https://doi.org/10.1016/j.jcou.2022.102292.

[8] Ren M, Ma T, Fang C, Liu X, Guo C, Zhang S, et al. Negative emission technology is key to decarbonizing China's cement industry. Appl Energy 2023;329:120254. https://doi.org/10.1016/j.apenergy.2022.120254.

[9] Verma YK, Ghime D, Mazumdar B, Ghosh P. Emission reduction through process integration and exploration of alternatives for sustainable clinker manufacturing. Int J Environ Sci Technol 2023. https://doi.org/10.1007/s13762-023-04754-7.

[10] Singh R, Sohal KS. Application of Waste Bones in Civil Engineering Practices. Sustain. Dev. Through Eng. Innov., 2021, p. 321–32. https://doi.org/10.1007/978-981-15-9554-7_28.

[11] Kapoor K, Singh SP, Singh B. Permeability of self-compacting concrete made with recycled concrete aggregates and Portland cement-fly ash-silica fume binder. J Sustain Cem Mater 2021;10:213–39. https://doi.org/10.1080/21650373.2020.1809029.

[12] Shrivas A, Jain D. Application of Different Waste in Concrete as a Partial Replacement of Cement Coarse Aggregate. Int J Sci Technol Eng 2015;2:89–107.

[13] Guney Y, Sari YD, Yalcin M, Tuncan A, Donmez S. Re-usage of waste foundry sand in high-strength concrete. Waste Manag 2010;30:1705–13. https://doi.org/10.1016/j.wasman.2010.02.018.

[14] Meyer C. Aerated Concrete as a Green Building Material. Aerated Concr 2006;1:10.

[15] Gopalakrishna B, Dinakar P. Mix design development of fly ash-GGBS based recycled aggregate geopolymer concrete. J Build Eng 2023;63:105551. https://doi.org/10.1016/j.jobe.2022.105551.

[16] Song Y, Zhao J, Ostrowski KA, Javed MF, Ahmad A, Khan MI, et al. Prediction of compressive strength of fly-ash-based concrete using ensemble and non-ensemble supervised machine-learning approaches. Appl Sci 2022;12. https://doi.org/10.3390/app12010361.

[17] Gardner L, Yun X, Walport F. The Continuous Strength Method – Review and outlook. Eng Struct 2023;275:114924. https://doi.org/10.1016/j.engstruct.2022.114924.

[18] Faried AS, Mostafa SA, Tayeh BA, Tawfik TA. Mechanical and durability properties of ultra-high performance concrete incorporated with various nano waste materials under different curing conditions. J Build Eng 2021;43:102569. https://doi.org/10.1016/j.jobe.2021.102569.

[19] Sandhu RK, Siddique R. Influence of rice husk ash (RHA) on the properties of self-compacting concrete: A review. Constr Build Mater 2017;153:751–64. https://doi.org/10.1016/j.conbuildmat.2017.07.165.

[20] Sohal KS, Singh R. Sustainable Use of Sugarcane Bagasse Ash in Concrete Production. In: Singh H, Cheema PPS, Garg P, editors. Sustain. Dev. Through Eng. Innov., 2020, p. 397–409.

[21] Kolawole JT, Babafemi AJ, Fanijo E, Chandra Paul S, Combrinck R. State-of-the-art review on the use of sugarcane bagasse ash in cementitious materials. Cem Concr Compos 2021;118:103975. https://doi.org/10.1016/j.cemconcomp.2021.103975.

[22] Singh R, Patel M. Investigating the Effect of Corn Cob Ash on the Characteristics of Cement Paste and Concrete: A Review. Environ. Concerns Remediat., Cham: Springer International Publishing; 2022, p. 91–103. https://doi.org/10.1007/978-3-031-05984-1_8.

[23] Adesanya DA. Evaluation of blended cement mortar , concrete and stabilized earth made from ordinary Portland cement and corn cob ash. Constr Build Mater Vol 1996;10:451–6.

[24] Singh R, Sodhi AK, Bhanot N. Sustainable Concrete Production by Integrating Wastes : A Comparative Study with and Without Bacillus Megaterium. Int. Conf. Sustain. Waste Manag. through Des., vol. 1, Springer International Publishing; 2019, p. 377–85. https://doi.org/10.1007/978-3-030-02707-0.

[25] Sohal KS, Kaur I, Singh R. Use of Electric Arc Furnace Dust in Concrete: A Review. Sustain. Waste Manag. through Des., 2019, p. 464–72. https://doi.org/10.1007/978-3-030-02707-0_53.

[26] Sodhi AK, Bhanot N, Singh R, Alkahtani M. Effect of integrating industrial and agricultural wastes on concrete performance with and without microbial activity. Environ Sci Pollut Res 2021:1–17.

[27] Singh R, Patel M. Strength and durability performance of rice straw ash-based concrete: an approach for the valorization of agriculture waste. Int J Environ Sci Technol 2022. https://doi.org/10.1007/s13762-022-04554-5.

[28] Ankur N, Singh N. Performance of cement mortars and concretes containing coal bottom ash: A comprehensive review. Renew Sustain Energy Rev 2021;149:111361. https://doi.org/10.1016/j.rser.2021.111361.

[29] Sua-Iam G, Makul N. Utilization of coal- and biomass-fired ash in the production of self-consolidating concrete: A literature review. J Clean Prod 2015;100:59–76. https://doi.org/10.1016/j.jclepro.2015.03.038.

[30] Singh R, Patel M, Sohal KS. The Potential Use of Waste Paper Sludge for Sustainable Production of Concrete—A Review. Recent Adv. Civ. Eng., 2022, p. 365–74. https://doi.org/10.1007/978-981-16-4396-5_33.

[31] Bui NK, Satomi T, Takahashi H. Influence of industrial by-products and waste paper sludge ash on properties of recycled aggregate concrete. J Clean Prod 2019;214:403–18. https://doi.org/10.1016/j.jclepro.2018.12.325.

[32] Williams A, Markandeya A, Stetsko Y, Riding K, Zayed A. Cracking potential and temperature sensitivity of metakaolin concrete. Constr Build Mater 2016;120:172–80. https://doi.org/10.1016/j.conbuildmat.2016.05.087.

[33] Dede T, Kankal M, Vosoughi AR, Grzywiński M, Kripka M. Artificial Intelligence Applications in Civil Engineering. Adv Civ Eng 2019;2019. https://doi.org/10.1155/2019/8384523.

[34] Minsky M. Steps Toward Artificial Intelligence. Proc IRE 1961;49:8–30. https://doi.org/10.1109/JRPROC.1961.287775.

[35] Lu P, Chen S, Zheng Y. Artificial Intelligence in Civil Engineering. Math Probl Eng 2012;2012:1–22. https://doi.org/10.1155/2012/145974.

[36] Marani A, Nehdi ML. Machine learning prediction of compressive strength for phase change materials integrated cementitious composites. Constr Build Mater 2020;265:120286. https://doi.org/10.1016/j.conbuildmat.2020.120286.

[37] Ahmad J, Zaid O, Siddique MS, Aslam F, Alabduljabbar H, Khedher KM. Mechanical and durability characteristics of sustainable coconut fibers reinforced concrete with incorporation of marble powder. Mater Res Express 2021;8. https://doi.org/10.1088/2053-1591/ac10d3.

[38] Farooq F, Amin MN, Khan K, Sadiq MR, Javed MF, Aslam F, et al. A comparative study of random forest and genetic engineering programming for the prediction of compressive strength of high strength concrete (HSC). Appl Sci 2020;10:1–18. https://doi.org/10.3390/app10207330.

[39] Song H, Ahmad A, Farooq F, Ostrowski KA, Maślak M, Czarnecki S, et al. Predicting the compressive strength of concrete with fly ash admixture using machine learning algorithms. Constr Build Mater 2021;308:1–15. https://doi.org/10.1016/j.conbuildmat.2021.125021.

[40] Yaseen ZM, Deo RC, Hilal A, Abd AM, Bueno LC, Salcedo-Sanz S, et al. Predicting compressive strength of lightweight foamed concrete using extreme learning machine model. Adv Eng Softw 2018;115:112–25. https://doi.org/10.1016/j.advengsoft.2017.09.004.

[41] Ashrafian A, Shokri F, Taheri Amiri MJ, Yaseen ZM, Rezaie-Balf M. Compressive strength of Foamed Cellular Lightweight Concrete simulation: New development of hybrid artificial intelligence model. Constr Build Mater 2020;230:117048. https://doi.org/10.1016/j.conbuildmat.2019.117048.

[42] Young BA, Hall A, Pilon L, Gupta P, Sant G. Can the compressive strength of concrete be estimated from knowledge of the mixture proportions?: New insights from statistical analysis and

machine learning methods. Cem Concr Res 2019;115:379–88. https://doi.org/10.1016/j.cemconres.2018.09.006.

[43] Al-Musawi AA, Alwanas AAH, Salih SQ, Ali ZH, Tran MT, Yaseen ZM. Shear strength of SFRCB without stirrups simulation: implementation of hybrid artificial intelligence model. Eng Comput 2020;36:1–11. https://doi.org/10.1007/s00366-018-0681-8.

[44] Yaseen ZM, Keshtegar B, Hwang H-J, Nehdi ML. Predicting reinforcing bar development length using polynomial chaos expansions. Eng Struct 2019;195:524–35. https://doi.org/10.1016/j.engstruct.2019.06.012.

[45] Liu B, Wei B, Li H, Mao Y. Multipoint hybrid model for RCC arch dam displacement health monitoring considering construction interface and its seepage. Appl Math Model 2022;110:674–97. https://doi.org/10.1016/j.apm.2022.06.023.

[46] Narendra BS, Sivapullaiah P V., Suresh S, Omkar SN. Prediction of unconfined compressive strength of soft grounds using computational intelligence techniques: A comparative study. Comput Geotech 2006;33:196–208. https://doi.org/10.1016/j.compgeo.2006.03.006.

[47] Ranjbar I, Toufigh V, Boroushaki M. A combination of deep learning and genetic algorithm for predicting the compressive strength of <scp>high-performance</scp> concrete. Struct Concr 2022;23:2405–18. https://doi.org/10.1002/suco.202100199.

[48] Ly H-B, Nguyen T-A, Thi Mai H-V, Tran VQ. Development of deep neural network model to predict the compressive strength of rubber concrete. Constr Build Mater 2021;301:124081. https://doi.org/10.1016/j.conbuildmat.2021.124081.

[49] SEEGER M. GAUSSIAN PROCESSES FOR MACHINE LEARNING. Int J Neural Syst 2004;14:69–106. https://doi.org/10.1142/S0129065704001899.

[50] Pham BT, Ly H-B, Al-Ansari N, Ho LS. A Comparison of Gaussian Process and M5P for Prediction of Soil Permeability Coefficient. Sci Program 2021;2021:1–13. https://doi.org/10.1155/2021/3625289.

[51] Muhammad A, Külahcı F, Salh H, Hama Rashid PA. Long Short Term Memory networks (LSTM)-Monte-Carlo simulation of soil ionization using radon. J Atmos Solar-Terrestrial Phys 2021;221:105688. https://doi.org/10.1016/j.jastp.2021.105688.

[52] Akan R, Keskin SN. The effect of data size of ANFIS and MLR models on prediction of unconfined compression strength of clayey soils. SN Appl Sci 2019;1:843. https://doi.org/10.1007/s42452-019-0883-8.

[53] Algaifi HA, Alqarni AS, Alyousef R, Bakar SA, Ibrahim MHW, Shahidan S, et al. Mathematical prediction of the compressive strength of bacterial concrete using gene expression programming. Ain Shams Eng J 2021;12:3629–39. https://doi.org/10.1016/j.asej.2021.04.008.

[54] Wan Z, Xu Y, Šavija B. On the Use of Machine Learning Models for Prediction of Compressive Strength of Concrete: Influence of Dimensionality Reduction on the Model Performance. Materials (Basel) 2021;14:713. https://doi.org/10.3390/ma14040713.

[55] Topçu İB, Sarıdemir M. Prediction of compressive strength of concrete containing fly ash using artificial neural networks and fuzzy logic. Comput Mater Sci 2008;41:305–11. https://doi.org/10.1016/j.commatsci.2007.04.009.

[56] Prasad BKR, Eskandari H, Reddy BVV. Prediction of compressive strength of SCC and HPC with high volume fly ash using ANN. Constr Build Mater 2009;23:117–28. https://doi.org/10.1016/j.conbuildmat.2008.01.014.

[57] Ahmad A, Farooq F, Niewiadomski P, Ostrowski K, Akbar A, Aslam F, et al. Prediction of compressive strength of fly ash based concrete using individual and ensemble algorithm. Materials (Basel) 2021;14:1–21. https://doi.org/10.3390/ma14040794.

[58] McCarthy MJ, Dhir RK. Development of high volume fly ash cements for use in concrete construction. Fuel 2005;84:1423–32. https://doi.org/10.1016/j.fuel.2004.08.029.

[59] Kayali MN, O. H. PROPERTIES OF HIGH-STRENGTH CONCRETE USING A FINE FLY ASH. Cem Concr Res 1998;28:1445–1452.

[60] Siddique R, Khatib JM. Abrasion resistance and mechanical properties of high-volume fly ash concrete. Mater Struct Constr 2010;43:709–18. https://doi.org/10.1617/s11527-009-9523-x.

[61] Thomas MDA. Optimizing the Use of Fly Ash in Concrete. 2007.

[62] Khambra G, Shukla P. Novel machine learning applications on fly ash based concrete: An overview. Mater Today Proc 2021. https://doi.org/10.1016/j.matpr.2021.07.262.

[63] Kavitha S, Varuna S, Ramya R. A comparative analysis on linear regression and support vector regression. Proc 2016 Online Int Conf Green Eng Technol IC-GET 2016 2017. https://doi.org/10.1109/GET.2016.7916627.

[64] Khambra G, Shukla P. Novel machine learning applications on fly ash based concrete: An overview. Mater Today Proc 2021. https://doi.org/10.1016/j.matpr.2021.07.262.

[65] Su X, Yan X, Tsai CL. Linear regression. Wiley Interdiscip Rev Comput Stat 2012;4:275–94. https://doi.org/10.1002/wics.1198.

[66] Charbuty B, Abdulazeez A. Classification Based on Decision Tree Algorithm for Machine Learning. J Appl Sci Technol Trends 2021;2:20–8. https://doi.org/10.38094/jastt20165.

[67] Myles AJ, Feudale RN, Liu Y, Woody NA, Brown SD. An introduction to decision tree modeling. J Chemom 2004;18:275–85. https://doi.org/10.1002/cem.873.

[68] Saxena R. How decision tree algorithm works. Dataaspirat 2017.

[69] Pisner DA, Schnyer DM. Support vector machine. Elsevier Inc.; 2019. https://doi.org/10.1016/B978-0-12-815739-8.00006-7.

[70] Yu H, Kim S. SVM Tutorial: Classification, Regression, and Ranking. vol. 1–4. 2012. https://doi.org/10.1007/978-3-540-92910-9.

[71] Noble WS. What is a support vector machine? Nat Biotechnol 2006;24:1565–7. https://doi.org/10.1038/nbt1206-1565.

[72] Chen T, Guestrin C. XGBoost: A Scalable Tree Boosting System. Proc. 22nd ACM SIGKDD Int. Conf. Knowl. Discov. Data Min., New York, NY, USA: ACM; 2016, p. 785–94. https://doi.org/10.1145/2939672.2939785.

[73] Pan B. Application of XGBoost algorithm in hourly PM2.5 concentration prediction. IOP Conf Ser Earth Environ Sci 2018;113:1–7. https://doi.org/10.1088/1755-1315/113/1/012127.

[74] Biau G, Scornet E. A random forest guided tour. Test 2016;25:197–227. https://doi.org/10.1007/s11749-016-0481-7.

[75] Qi C, Huang B, Wu M, Wang K, Yang S, Li G. Concrete Strength Prediction Using Different Machine Learning Processes: Effect of Slag, Fly Ash and Superplasticizer. Materials (Basel) 2022;15. https://doi.org/10.3390/ma15155369.

[76] Khan MA, Memon SA, Farooq F, Javed MF, Aslam F, Alyousef R. Compressive Strength of Fly-Ash-Based Geopolymer Concrete by Gene Expression Programming and Random Forest. Adv Civ Eng 2021;2021. https://doi.org/10.1155/2021/6618407.

[77] Khan GM. Artificial neural network (ANNs). Stud Comput Intell 2018;725:39–55. https://doi.org/10.1007/978-3-319-67466-7_4.

[78] Agrawal SK. Understanding the Basics Of Artificial Neural Network,. Data Sci Blogathon, Anal Vidhya, 2021.

[79] Ahmad A, Ostrowski KA, Maślak M, Farooq F, Mehmood I, Nafees A. Comparative study of supervised machine learning algorithms for predicting the compressive strength of concrete at high temperature. Materials (Basel) 2021;14. https://doi.org/10.3390/ma14154222.

[80] Gardner M., Dorling S. Artificial neural networks (the multilayer perceptron)—a review of applications in the atmospheric sciences. Atmos Environ 1998;32:2627–36. https://doi.org/10.1016/S1352-2310(97)00447-0.

[81] Umeonyiagu I, Nwobi-Okoye C. Predicting Flexural Strength of Concretes Incorporating River Gravel Using Multi-Layer Perceptron Networks: A Case Study of Eastern Nigeria. Niger J Technol 2014;34:12. https://doi.org/10.4314/njt.v34i1.2.

[82] SINGH B, SINGH B, SIHAG P, TOMAR A, SEHGAL A. Estimation of compressive strength of high-strength concrete by random forest and M5P model tree approaches. J Mater Eng Struct « JMES » 2019;6:583–92.

[83] Jo H-S, Park C, Lee E, Choi HK, Park J. Path Loss Prediction Based on Machine Learning Techniques: Principal Component Analysis, Artificial Neural Network, and Gaussian Process. Sensors 2020;20:1927. https://doi.org/10.3390/s20071927.

[84] Bouzoubaa N, Zhang MH, Bilodeau A, Malhotra VM. Mechanical properties and durability of concrete made with high volume Fly ash blended cements. Cem Concr Compos 1998;SP178:575–603.

[85] Nochaiya T, Wongkeo W, Chaipanich A. Utilization of fly ash with silica fume and properties of Portland cement-fly ash-silica fume concrete. Fuel 2010;89:768–74. https://doi.org/10.1016/j.fuel.2009.10.003.

[86] Atis CD. High-Volume Fly Ash Concrete with High Strength and Low Drying Shrinkage. J Mater Civ Eng 2003;15:153–6. https://doi.org/10.1061/(asce)0899-1561(2003)15:2(153).

[87] Kumar B, Tike GK, Nanda PK. Evaluation of Properties of High-Volume Fly-Ash Concrete. J Mater Civ Eng 2007:906–12.

[88] Oner A, Akyuz S, Yildiz R. An experimental study on strength development of concrete containing fly ash and optimum usage of fly ash in concrete. Cem Concr Res 2005;35:1165–71. https://doi.org/10.1016/j.cemconres.2004.09.031.

[89] Moffatt EG, Thomas MDA, Fahim A. Performance of high-volume fly ash concrete in marine environment. Cem Concr Res 2017;102:127–35. https://doi.org/10.1016/j.cemconres.2017.09.008.

[90] Khatib JM. Performance of self-compacting concrete containing fly ash. Constr Build Mater 2008;22:1963–71. https://doi.org/10.1016/j.conbuildmat.2007.07.011.

[91] Barbhuiya SA, Gbagbo JK, Russell MI, Basheer PAM. Properties of fly ash concrete modified with hydrated lime and silica fume. Constr Build Mater 2009;23:3233–9. https://doi.org/10.1016/j.conbuildmat.2009.06.001.

[92] Reiner M, Rens K. High-Volume Fly Ash Concrete: Analysis and Application. Pract Period Struct Des Constr 2006;11:58–64. https://doi.org/10.1061/(asce)1084-0680(2006)11:1(58).

[93] Rivera F, Martínez P, Castro J, López M. Massive volume fly-ash concrete: A more sustainable material with fly ash replacing cement and aggregates. Cem Concr Compos 2015;63:104–12. https://doi.org/10.1016/j.cemconcomp.2015.08.001.

[94] Li G. A new way to increase the long-term bond strength of new-to-old concrete by the use of fly ash. Cem Concr Res 2003;33:799–806. https://doi.org/10.1016/S0008-8846(02)01064-5.

[95] Babu KG, Rao GSN. EFFICIENCY OF FLY ASH IN CONCRETE WITH AGE. Cem Concr Res 1996;26:465–76.

[96] Cao C, Sun W, Qin H. The Analysis on strength and fly ash effect of roller-compacted concrete with high volume fly ash. Cem Concr Res 2000;30:71–5. https://doi.org/10.1016/S0008-8846(99)00203-3.

[97] Ravina D, Mehta PK. COMPRESSIVE STRENGTH OF LOW CEMENT / HIGH FLY ASH CONCRETE. Cem Concr Res 1988;18:571–83.

[98] Golewski GL. Effect of curing time on the fracture toughness of fly ash concrete composites. Compos Struct 2018;185:105–12. https://doi.org/10.1016/j.compstruct.2017.10.090.

[99] Herath C, Gunasekara C, Law DW, Setunge S. Performance of high volume fly ash concrete incorporating additives: A systematic literature review. Constr Build Mater 2020;258:120606. https://doi.org/10.1016/j.conbuildmat.2020.120606.

[100] Montgomery DG. FLY ASH IN CONCRETE - A MICROSTEUCTURE STUDY. Cem Concr Res 1981;11:591–603.

[101] Slanicka. THE INFLUENCE OF FLY ASH FINEEESS ON THE STRENGTH OF CONCRETE. Cem Concr Res 1991;21:285–96.

[102] Gopalan MK. Sorptivity of Fly Ash Concretes. Cem Concr Res 1996;26:1189–97.

[103] Bouzoubaâ N, Lachemi M. Self-compacting concrete incorporating high volumes of class F fly ash. Cem Concr Res 2001;31:413–20. https://doi.org/10.1016/S0008-8846(00)00504-4.

[104] Kayali O. Fly ash lightweight aggregates in high performance concrete. Constr Build Mater 2008;22:2393–9. https://doi.org/10.1016/j.conbuildmat.2007.09.001.

[105] Kang S, Lloyd Z, Kim T, Ley MT. Predicting the compressive strength of fly ash concrete with the Particle Model. Cem Concr Res 2020;137:106218. https://doi.org/10.1016/j.cemconres.2020.106218.

[106] Rai P, Qiu W, Pei H, Chen J, Ai X, Liu Y, et al. Effect of Fly Ash and Cement on the Engineering Characteristic of Stabilized Subgrade Soil: An Experimental Study. Geofluids 2021;2021. https://doi.org/10.1155/2021/1368194.

[107] Venkateswara Rao A, Srinivasa Rao K. Effect of fly ash on strength of concrete. Circ Econ Fly Ash Manag 2019;14:125–34. https://doi.org/10.1007/978-981-15-0014-5_9.

[108] Malhotra VM. Durability of concrete incorporating high-volume of low-calcium (ASTM Class F) fly ash. Cem Concr Compos 1990;12:271–7. https://doi.org/10.1016/0958-9465(90)90006-J.

[109] Sun J, Shen X, Tan G, Tanner JE. Compressive strength and hydration characteristics of high-volume fly ash concrete prepared from fly ash. J Therm Anal Calorim 2019;136:565–80. https://doi.org/10.1007/s10973-018-7578-z.

[110] mike yi. A Complete Guide to Scatter Plots. Data Tutorials 2021.

[111] Wang Y, Han F, Zhu L, Deussen O, Chen B. Line Graph or Scatter Plot? Automatic Selection of Methods for Visualizing Trends in Time Series. IEEE Trans Vis Comput Graph 2018;24:1141–54. https://doi.org/10.1109/TVCG.2017.2653106.

[112] V. DD, Fischer RL, Fogelson DE. Prediction of compressive strength from other rock properties (Vol. 6702). US Dep. Inter. Bur. Mines., 1965.

[113] Dauji S. Neural prediction of concrete compressive strength. Int J Mater Struct Integr 2018;12:17–35. https://doi.org/10.1504/IJMSI.2018.093884.

[114] Chen N, Zhao S, Gao Z, Wang D, Liu P, Oeser M, et al. Virtual mix design: Prediction of compressive strength of concrete with industrial wastes using deep data augmentation. Constr Build Mater 2022;323:126580. https://doi.org/10.1016/j.conbuildmat.2022.126580.

[115] Asteris PG, Skentou AD, Bardhan A, Samui P, Pilakoutas K. Predicting concrete compressive strength using hybrid ensembling of surrogate machine learning models. Cem Concr Res 2021;145:106449. https://doi.org/10.1016/j.cemconres.2021.106449.

[116] Marani A, Jamali A, Nehdi ML. Predicting Ultra-High-Performance Concrete Compressive Strength Using Tabular Generative Adversarial Networks. Materials (Basel) 2020;13:4757. https://doi.org/10.3390/ma13214757.

[117] Kumar Tipu R, Panchal VR, Pandya KS. An ensemble approach to improve BPNN model precision for predicting compressive strength of high-performance concrete. Structures 2022;45:500–8. https://doi.org/10.1016/j.istruc.2022.09.046.

[118] Gupta P, Gupta N, Saxena KK, Goyal S. Multilayer perceptron modelling of geopolymer composite incorporating fly ash and GGBS for prediction of compressive strength. Adv Mater Process Technol 2022;8:1441–55. https://doi.org/10.1080/2374068X.2021.1946751.

[119] Ma Q, Li J, Aamer M, Huang G. Effect of Chinese milk vetch (astragalus sinicus l.) and rice straw incorporated in paddy soil on greenhouse gas emission and soil properties. Agronomy 2020;10. https://doi.org/10.3390/agronomy10050717.

[120] Naser AH, Badr AH, Henedy SN, Ostrowski KA, Imran H. Application of Multivariate Adaptive Regression Splines (MARS) approach in prediction of compressive strength of eco-friendly concrete. Case Stud Constr Mater 2022;17:e01262. https://doi.org/10.1016/j.cscm.2022.e01262.

[121] Akshita chugh. MAE, MSE, RMSE, Coefficient of Determination, Adjusted R Squared — Which Metric is Better? Anal Vidhya 2020.

[122] Seif G. Understanding the 3 most common loss functions for Machine Learning Regression. Towar Data Sci 2019.

[123] Zhang X, Akber MZ, Zheng W. Prediction of seven-day compressive strength of field concrete. Constr Build Mater 2021;305:124604. https://doi.org/10.1016/j.conbuildmat.2021.124604.

[124] Amin MN, Al-Hashem MN, Ahmad A, Khan K, Ahmad W, Qadir MG, et al. Application of Soft-Computing Methods to Evaluate the Compressive Strength of Self-Compacting Concrete. Materials (Basel) 2022;15:7800. https://doi.org/10.3390/ma15217800.

[125] FERNANDO J. R-Squared. Investopedia 2021.

[126] Kamalov F. Sensitivity Analysis for Feature Selection. Proc - 17th IEEE Int Conf Mach Learn Appl ICMLA 2018 2019:1466–70. https://doi.org/10.1109/ICMLA.2018.00238.

[127] Arachchilage CB, Fan C, Zhao J, Huang G, Liu WV. A machine learning model to predict unconfined compressive strength of alkali-activated slag-based cemented paste backfill. J Rock Mech Geotech Eng 2023. https://doi.org/10.1016/j.jrmge.2022.12.009.

[128] Taylor KE. Summarizing multiple aspects of model performance in a single diagram. J Geophys Res Atmos 2001;106:7183–92. https://doi.org/10.1029/2000JD900719.

[129] Pandey M, Jamei M, Ahmadianfar I, Karbasi M, Lodhi AS, Chu X. Assessment of scouring around submerged spur dike in cohesive sediment mixtures: A comparative study on three rigorous machine learning models. J Hydrol 2021:127330. https://doi.org/10.1016/j.jhydrol.2021.127330.

[130] Yesiloglu-Gultekin N, Gokceoglu C. A Comparison Among Some Non-linear Prediction Tools on Indirect Determination of Uniaxial Compressive Strength and Modulus of Elasticity of Basalt. J Nondestruct Eval 2022;41:10. https://doi.org/10.1007/s10921-021-00841-2.

[131] Gupta S, Sihag P. Prediction of the compressive strength of concrete using various predictive modeling techniques. Neural Comput Appl 2022;34:6535–45. https://doi.org/10.1007/s00521-021-06820-y.

Annexure 1

W/c ratio	Cement Content	Fine Aggregate	Coarse Aggregate	Water content	SiO_2	CaO	Fe_2O_3	Al_2O_3	Specific Gravity	Curing Days	Replacement Percentage	Compressive Strength
0.32	168	701	1052	120	62.6	5.8	4.5	20.9	2.01	1	50	7.7
0.4	385	729	1094	154	62.6	5.8	4.5	20.9	2.01	1	0	21.4
0.42	389	729	1093	164	62.6	5.8	4.5	20.9	2.01	1	0	30.5
0.32	168	701	1052	120	62.6	5.8	4.5	20.9	2.01	7	50	15.9
0.32	170	710	1066	122	62.6	5.8	4.5	20.9	2.01	7	50	20.9
0.32	391	740	1111	125	62.6	5.8	4.5	20.9	2.01	7	-	30.5
0.4	385	729	1094	154	62.6	5.8	4.5	20.9	2.01	7	0	32.5
0.42	389	729	1093	164	62.6	5.8	4.5	20.9	2.01	7	0	39.1
0.32	168	701	1052	120	62.6	5.8	4.5	20.9	2.01	14	50	19.6
0.32	170	710	1066	122	62.6	5.8	4.5	20.9	2.01	14	50	27.1
0.32	391	740	1111	125	62.6	5.8	4.5	20.9	2.01	14	-	37.5
0.4	385	729	1094	154	62.6	5.8	4.5	20.9	2.01	14	0	34.4
0.42	389	729	1093	164	62.6	5.8	4.5	20.9	2.01	14	0	41
0.32	168	701	1052	120	62.6	5.8	4.5	20.9	2.01	28	50	24
0.32	170	710	1066	122	62.6	5.8	4.5	20.9	2.01	28	50	30.5
0.32	391	740	1111	125	62.6	5.8	4.5	20.9	2.01	28	-	43.8
0.32	391	740	1111	125	62.6	5.8	4.5	20.9	2.01	28	-	43.3
0.4	385	729	1094	154	62.6	5.8	4.5	20.9	2.01	28	0	38.6
0.4	385	729	1094	154	62.6	5.8	4.5	20.9	2.01	28	0	38.8
0.42	389	729	1093	164	62.6	5.8	4.5	20.9	2.01	28	0	46.3
0.42	384	720	1081	162	62.6	5.8	4.5	20.9	2.01	28	0	42.1
0.32	168	701	1052	120	62.6	5.8	4.5	20.9	2.01	91	50	32.7
0.32	170	710	1066	122	62.6	5.8	4.5	20.9	2.01	91	50	41.6
0.32	391	740	1111	125	62.6	5.8	4.5	20.9	2.01	91	-	53.7
0.4	385	729	1094	154	62.6	5.8	4.5	20.9	2.01	91	-	43.4
0.42	389	729	1093	164	62.6	5.8	4.5	20.9	2.01	91	0	50.4
0.32	168	701	1052	120	62.6	5.8	4.5	20.9	2.01	365	50	40.3
0.32	170	710	1066	122	62.6	5.8	4.5	20.9	2.01	365	50	61.9
0.5	336	739	1105	167	52.4	13.4	4.7	23.4	2.08	1	0	16.7
0.45	247	845	846	186	52.4	13.4	4.7	23.4	2.08	1	40	8.7

0.4	238	844	844	189	52.4	13.4	4.7	23.4	2.08	1	40	10.7
0.35	232	846	847	136	52.4	13.4	4.7	23.4	2.08	1	40	16.6
0.45	207	845	843	188	52.4	13.4	4.7	23.4	2.08	1	50	6.1
0.4	200	842	843	161	52.4	13.4	4.7	23.4	2.08	1	50	7
0.35	197	856	856	138	52.4	13.4	4.7	23.4	2.08	1	50	7.8
0.45	169	833	853	190	52.4	13.4	4.7	23.4	2.08	1	60	5.2
0.4	163	851	851	164	52.4	13.4	4.7	23.4	2.08	1	60	4.9
0.35	161	866	864	141	52.4	13.4	4.7	23.4	2.08	1	60	7.3
0.5	336	739	1105	167	52.4	13.4	4.7	23.4	2.08	7	0	27.3
0.45	247	845	846	186	52.4	13.4	4.7	23.4	2.08	7	40	21.2
0.4	238	844	844	189	52.4	13.4	4.7	23.4	2.08	7	40	25.8
0.35	232	846	847	136	52.4	13.4	4.7	23.4	2.08	7	40	31.3
0.45	207	845	843	188	52.4	13.4	4.7	23.4	2.08	7	50	17.4
0.4	200	842	843	161	52.4	13.4	4.7	23.4	2.08	7	50	19.3
0.35	197	856	856	138	52.4	13.4	4.7	23.4	2.08	7	50	22.9
0.45	169	833	853	190	52.4	13.4	4.7	23.4	2.08	7	60	15.6
0.4	163	851	851	164	52.4	13.4	4.7	23.4	2.08	7	60	14.7
0.35	161	866	864	141	52.4	13.4	4.7	23.4	2.08	7	60	20.6
0.5	336	739	1105	167	52.4	13.4	4.7	23.4	2.08	28	0	34.6
0.45	247	845	846	186	52.4	13.4	4.7	23.4	2.08	28	40	34.6
0.4	238	844	844	189	52.4	13.4	4.7	23.4	2.08	28	40	37.8
0.35	232	846	847	136	52.4	13.4	4.7	23.4	2.08	28	40	48.3
0.45	207	845	843	188	52.4	13.4	4.7	23.4	2.08	28	50	33.2
0.4	200	842	843	161	52.4	13.4	4.7	23.4	2.08	28	50	34.9
0.35	197	856	856	138	52.4	13.4	4.7	23.4	2.08	28	50	28.9
0.45	169	833	853	190	52.4	13.4	4.7	23.4	2.08	28	60	30.2
0.4	163	851	851	164	52.4	13.4	4.7	23.4	2.08	28	60	26.2
0.35	161	866	864	141	52.4	13.4	4.7	23.4	2.08	28	60	35.8
0.64	300	0	0	193	58.2	1.6	4	28.5	2.28	7	0	38.8
0.64	300	0	0	193	58.2	1.6	4	28.5	2.28	28	0	62.9
0.31	231	852	1047	119	32.2	31.9	5.6	18.1	2.58	1	40	17
0.3	195	854	1041	120	34.9	27.6	6.2	19.6	2.62	1	50	7
0.3	156	834	1026	121	30.9	31.4	5.2	18.3	2.68	1	60	0.8
0.3	229	827	1040	115	32.2	31.9	5.6	18.1	2.58	1	40	9.7
0.29	193	836	1032	114	34.9	27.6	6.2	19.6	2.62	1	50	4.8
0.3	155	842	1016	116	30.9	31.4	5.2	18.3	2.68	1	60	2.3

0.3	229	844	1032	113	32.2	31.9	5.6	18.1	2.58	1	40	16.4
0.3	193	850	1126	116	34.9	27.6	6.2	19.6	2.62	1	50	13.1
0.3	154	818	1016	117	30.9	31.4	5.2	18.3	2.68	1	60	6.9
0.31	368	886	1085	115	-	-	-	-	-	7	0	40.3
0.31	231	852	1047	119	32.2	31.9	5.6	18.1	2.58	7	40	42.8
0.3	195	854	1041	120	34.9	27.6	6.2	19.6	2.62	7	50	34.3
0.3	156	834	1026	121	30.9	31.4	5.2	18.3	2.68	7	60	26.9
0.3	229	827	1040	115	32.2	31.9	5.6	18.1	2.58	7	40	32.6
0.29	193	836	1032	114	34.9	27.6	6.2	19.6	2.62	7	50	23.4
0.3	155	842	1016	116	30.9	31.4	5.2	18.3	2.68	7	60	22.1
0.3	229	844	1032	113	32.2	31.9	5.6	18.1	2.58	7	40	37.7
0.3	193	850	1126	116	34.9	27.6	6.2	19.6	2.62	7	50	33.9
0.3	154	818	1016	117	30.9	31.4	5.2	18.3	2.68	7	60	25.8
0.31	368	886	1085	115	-	-	-	-	-	28	0	48.6
0.31	231	852	1047	119	32.2	31.9	5.6	18.1	2.58	28	40	55.3
0.3	195	854	1041	120	34.9	27.6	6.2	19.6	2.62	28	50	44
0.3	156	834	1026	121	30.9	31.4	5.2	18.3	2.68	28	60	43.7
0.3	229	827	1040	115	32.2	31.9	5.6	18.1	2.58	28	40	44.6
0.29	193	836	1032	114	34.9	27.6	6.2	19.6	2.62	28	50	36.8
0.3	155	842	1016	116	30.9	31.4	5.2	18.3	2.68	28	60	28.6
0.3	229	844	1032	113	32.2	31.9	5.6	18.1	2.58	28	40	46.3
0.3	193	850	1126	116	34.9	27.6	6.2	19.6	2.62	28	50	42.2
0.3	154	818	1016	117	30.9	31.4	5.2	18.3	2.68	28	60	40
0.31	368	886	1085	115	-	-	-	-	-	91	0	53
0.31	231	852	1047	119	32.2	31.9	5.6	18.1	2.58	91	40	67.9
0.3	195	854	1041	120	34.9	27.6	6.2	19.6	2.62	91	50	51.2
0.3	156	834	1026	121	30.9	31.4	5.2	18.3	2.68	91	60	54.4
0.3	229	827	1040	115	32.2	31.9	5.6	18.1	2.58	91	40	52.9
0.29	193	836	1032	114	34.9	27.6	6.2	19.6	2.62	91	50	43.4
0.3	155	842	1016	116	30.9	31.4	5.2	18.3	2.68	91	60	41.9
0.3	229	844	1032	113	32.2	31.9	5.6	18.1	2.58	91	40	51.1
0.3	193	850	1126	116	34.9	27.6	6.2	19.6	2.62	91	50	51.3
0.3	154	818	1016	117	30.9	31.4	5.2	18.3	2.68	91	60	44.2
0.31	368	886	1085	115						365	0	66.5
0.31	231	852	1047	119	32.2	31.9	5.6	18.1	2.58	365	40	72.5
0.3	195	854	1041	120	34.9	27.6	6.2	19.6	2.62	365	50	66.9

0.3	156	834	1026	121	30.9	31.4	5.2	18.3	2.68	365	60	60.8
0.3	229	827	1040	115	32.2	31.9	5.6	18.1	2.58	365	40	63.3
0.29	193	836	1032	114	34.9	27.6	6.2	19.6	2.62	365	50	55.1
0.3	155	842	1016	116	30.9	31.4	5.2	18.3	2.68	365	60	52.9
0.3	229	844	1032	113	32.2	31.9	5.6	18.1	2.58	365	40	62.9
0.3	154	818	1016	117	30.9	31.4	5.2	18.3	2.68	365	60	55.7
0.31	155	616	1264	114	55.6	12.3	3.48	23.1	-	28	33.2	
0.45	409	829	1026	184	59.15	5.93	3.85	21.63	-	3	0	36.5
0.45	249.4	829	1026	184	59.15	5.93	3.85	21.63	-	3	40	20.3
0.45	184.1	829	1026	184	59.15	5.93	3.85	21.63	-	3	55	12.1
0.45	122.7	829	1026	184	59.15	5.93	3.85	21.63	-	3	60	4.7
0.45	409	829	1026	184	59.15	5.93	3.85	21.63	-	7	0	40.5
0.45	249.4	829	1026	184	59.15	5.93	3.85	21.63	-	7	40	24.3
0.45	184.1	829	1026	184	59.15	5.93	3.85	21.63	-	7	55	15
0.45	122.7	829	1026	184	59.15	5.93	3.85	21.63	-	7	60	6.7
0.45	409	829	1026	184	59.15	5.93	3.85	21.63	-	28	0	47.8
0.45	249.4	829	1026	184	59.15	5.93	3.85	21.63	-	28	40	39.6
0.45	184.1	829	1026	184	59.15	5.93	3.85	21.63	-	28	55	26.5
0.45	122.7	829	1026	184	59.15	5.93	3.85	21.63	-	28	60	11.5
0.45	409	829	1026	184	59.15	5.93	3.85	21.63	-	56	0	50.7
0.45	249.4	829	1026	184	59.15	5.93	3.85	21.63	-	56	40	48.3
0.45	184.1	829	1026	184	59.15	5.93	3.85	21.63	-	56	55	34.4
0.45	122.7	829	1026	184	59.15	5.93	3.85	21.63	-	56	60	16
0.45	409	829	1026	184	59.15	5.93	3.85	21.63	-	90	0	52.5
0.45	249.4	829	1026	184	59.15	5.93	3.85	21.63	-	90	40	51.1
0.45	184.1	829	1026	184	59.15	5.93	3.85	21.63	-	90	55	41.2
0.45	122.7	829	1026	184	59.15	5.93	3.85	21.63	-	90	60	28.1
0.56	360	616	410	25.1	39.8	15.2	13.7	21.5	-	28	0	43.2
0.56	322	611	408	23.9	39.8	15.2	13.7	21.5	-	28	10	41.5
0.56	320	607	404	25.4	39.8	15.2	13.7	21.5	-	28	10	46.2
0.56	284	607	405	23.3	39.8	15.2	13.7	21.5	-	28	20	37.5
0.56	280	598	398	26	39.8	15.2	13.7	21.5	-	28	20	43
0.56	247	604	402	22.7	39.8	15.2	13.7	21.5	-	28	30	33.5
0.56	243	594	396	25	39.8	15.2	13.7	21.5	-	28	30	36.5
0.34	400	600	1200	136	50.2	2.6	13.2	28.6	2.4	1	0	12.05
0.32	400	600	1200	128	50.2	2.6	13.2	28.6	2.4	1	0	33.51

0.28	120	600	1200	112	50.2	2.6	13.2	28.6	2.4	1	70	1.76
0.29	120	600	1200	116	50.2	2.6	13.2	28.6	2.4	1	70	7.09
0.33	200	600	1200	132	50.2	2.6	13.2	28.6	2.4	1	50	5.62
0.3	200	600	1200	120	50.2	2.6	13.2	28.6	2.4	1	50	28.25
0.34	400	600	1200	136	50.2	2.6	13.2	28.6	2.4	3	0	38.41
0.32	400	600	1200	128	50.2	2.6	13.2	28.6	2.4	3	0	45.27
0.28	120	600	1200	112	50.2	2.6	13.2	28.6	2.4	3	70	16.34
0.29	120	600	1200	116	50.2	2.6	13.2	28.6	2.4	3	70	16.64
0.33	200	600	1200	132	50.2	2.6	13.2	28.6	2.4	3	50	31.85
0.3	200	600	1200	120	50.2	2.6	13.2	28.6	2.4	3	50	35.3
0.34	400	600	1200	136	50.2	2.6	13.2	28.6	2.4	7	0	49.27
0.32	400	600	1200	128	50.2	2.6	13.2	28.6	2.4	7	0	52.63
0.28	120	600	1200	112	50.2	2.6	13.2	28.6	2.4	7	70	24.01
0.29	120	600	1200	116	50.2	2.6	13.2	28.6	2.4	7	70	18.6
0.33	200	600	1200	132	50.2	2.6	13.2	28.6	2.4	7	50	38
0.3	200	600	1200	120	50.2	2.6	13.2	28.6	2.4	7	50	48.3
0.34	400	600	1200	136	50.2	2.6	13.2	28.6	2.4	28	0	60.75
0.32	400	600	1200	128	50.2	2.6	13.2	28.6	2.4	28	0	64.95
0.28	120	600	1200	112	50.2	2.6	13.2	28.6	2.4	28	70	33.25
0.29	120	600	1200	116	50.2	2.6	13.2	28.6	2.4	28	70	30.55
0.33	200	600	1200	132	50.2	2.6	13.2	28.6	2.4	28	50	57
0.3	200	600	1200	120	50.2	2.6	13.2	28.6	2.4	28	50	66.55
0.34	400	600	1200	136	50.2	2.6	13.2	28.6	2.4	91	0	65.03
0.32	400	600	1200	128	50.2	2.6	13.2	28.6	2.4	91	0	68.1
0.28	120	600	1200	112	50.2	2.6	13.2	28.6	2.4	91	70	40.75
0.29	120	600	1200	116	50.2	2.6	13.2	28.6	2.4	91	70	41.1
0.33	200	600	1200	132	50.2	2.6	13.2	28.6	2.4	91	50	60.2
0.3	200	600	1200	120	50.2	2.6	13.2	28.6	2.4	91	50	79
0.34	400	600	1200	136	50.2	2.6	13.2	28.6	2.4	180	0	69.13
0.32	400	600	1200	128	50.2	2.6	13.2	28.6	2.4	180	0	72.29
0.28	120	600	1200	112	50.2	2.6	13.2	28.6	2.4	180	70	42.25
0.29	120	600	1200	116	50.2	2.6	13.2	28.6	2.4	180	70	43
0.33	200	600	1200	132	50.2	2.6	13.2	28.6	2.4	180	50	67.3
0.3	200	600	1200	120	50.2	2.6	13.2	28.6	2.4	180	50	81.6
0.34	400	600	1200	136	50.2	2.6	13.2	28.6	2.4	365	0	71
0.32	400	600	1200	128	50.2	2.6	13.2	28.6	2.4	365	0	77.08

0.28	120	600	1200	112	50.2	2.6	13.2	28.6	2.4	365	70	45
0.29	120	600	1200	116	50.2	2.6	13.2	28.6	2.4	365	70	48.05
0.33	200	600	1200	132	50.2	2.6	13.2	28.6	2.4	365	50	67.6
0.3	200	600	1200	120	50.2	2.6	13.2	28.6	2.4	365	50	83.6
0.4	400	585	1270	160	62.54	1.54	4.98	28	2.4	7	0	3.56
0.4	320	564	1270	160	62.54	1.54	4.98	28	2.4	7	20	3.38
0.4	280	554	1270	160	62.54	1.54	4.98	28	2.4	7	30	3.06
0.4	240	543	1270	160	62.54	1.54	4.98	28	2.4	7	40	2.81
0.4	200	533	1270	160	62.54	1.54	4.98	28	2.4	7	50	2.64
0.4	160	522	1270	160	62.54	1.54	4.98	28	2.4	7	60	2.48
0.34	400	649	1270	136	62.54	1.54	4.98	28	2.4	7	0	4.16
0.34	320	628	1270	136	62.54	1.54	4.98	28	2.4	7	20	4.26
0.34	280	618	1270	136	62.54	1.54	4.98	28	2.4	7	30	3.78
0.34	240	607	1270	136	62.54	1.54	4.98	28	2.4	7	40	3.25
0.34	200	596	1270	136	62.54	1.54	4.98	28	2.4	7	50	2.98
0.34	160	586	1270	136	62.54	1.54	4.98	28	2.4	7	60	2.84
0.3	400	692	1270	120	62.54	1.54	4.98	28	2.4	7	0	4.31
0.3	320	671	1270	120	62.54	1.54	4.98	28	2.4	7	20	4.49
0.3	280	660	1270	120	62.54	1.54	4.98	28	2.4	7	30	3.86
0.3	240	650	1270	120	62.54	1.54	4.98	28	2.4	7	40	3.65
0.3	200	639	1270	120	62.54	1.54	4.98	28	2.4	7	50	3.5
0.3	160	628	1270	120	62.54	1.54	4.98	28	2.4	7	60	3.4
0.4	400	585	1270	160	62.54	1.54	4.98	28	2.4	28	0	4.5
0.4	320	564	1270	160	62.54	1.54	4.98	28	2.4	28	20	4.32
0.4	280	554	1270	160	62.54	1.54	4.98	28	2.4	28	30	4.26
0.4	240	543	1270	160	62.54	1.54	4.98	28	2.4	28	40	4.19
0.4	200	533	1270	160	62.54	1.54	4.98	28	2.4	28	50	3.82
0.4	160	522	1270	160	62.54	1.54	4.98	28	2.4	28	60	3.64
0.34	400	649	1270	136	62.54	1.54	4.98	28	2.4	28	0	5.11
0.34	320	628	1270	136	62.54	1.54	4.98	28	2.4	28	20	5.17
0.34	280	618	1270	136	62.54	1.54	4.98	28	2.4	28	30	4.81
0.34	240	607	1270	136	62.54	1.54	4.98	28	2.4	28	40	4.78
0.34	200	596	1270	136	62.54	1.54	4.98	28	2.4	28	50	4.48
0.34	160	586	1270	136	62.54	1.54	4.98	28	2.4	28	60	4.19
0.3	400	692	1270	120	62.54	1.54	4.98	28	2.4	28	0	5.65
0.3	320	671	1270	120	62.54	1.54	4.98	28	2.4	28	20	6

0.3	280	660	1270	120	62.54	1.54	4.98	28	2.4	28	30	5.62
0.3	240	650	1270	120	62.54	1.54	4.98	28	2.4	28	40	5.47
0.3	200	639	1270	120	62.54	1.54	4.98	28	2.4	28	50	5.28
0.3	160	628	1270	120	62.54	1.54	4.98	28	2.4	28	60	4.75
0.4	400	585	1270	160	62.54	1.54	4.98	28	2.4	90	0	4.79
0.4	320	564	1270	160	62.54	1.54	4.98	28	2.4	90	20	4.72
0.4	280	554	1270	160	62.54	1.54	4.98	28	2.4	90	30	4.89
0.4	240	543	1270	160	62.54	1.54	4.98	28	2.4	90	40	4.95
0.4	200	533	1270	160	62.54	1.54	4.98	28	2.4	90	50	4.61
0.4	160	522	1270	160	62.54	1.54	4.98	28	2.4	90	60	4.44
0.34	400	649	1270	136	62.54	1.54	4.98	28	2.4	90	0	5.51
0.34	320	628	1270	136	62.54	1.54	4.98	28	2.4	90	20	5.6
0.34	280	618	1270	136	62.54	1.54	4.98	28	2.4	90	30	5.74
0.34	240	607	1270	136	62.54	1.54	4.98	28	2.4	90	40	5.81
0.34	200	596	1270	136	62.54	1.54	4.98	28	2.4	90	50	5.43
0.34	160	586	1270	136	62.54	1.54	4.98	28	2.4	90	60	4.92
0.3	400	692	1270	120	62.54	1.54	4.98	28	2.4	90	0	6.37
0.3	320	671	1270	120	62.54	1.54	4.98	28	2.4	90	20	6.35
0.3	280	660	1270	120	62.54	1.54	4.98	28	2.4	90	30	6.4
0.3	240	650	1270	120	62.54	1.54	4.98	28	2.4	90	40	6.57
0.3	200	639	1270	120	62.54	1.54	4.98	28	2.4	90	50	5.86
0.3	160	628	1270	120	62.54	1.54	4.98	28	2.4	90	60	5.25
0.4	400	585	1270	160	62.54	1.54	4.98	28	2.4	180	0	5.26
0.4	320	564	1270	160	62.54	1.54	4.98	28	2.4	180	20	5.44
0.4	280	554	1270	160	62.54	1.54	4.98	28	2.4	180	30	5.49
0.4	240	543	1270	160	62.54	1.54	4.98	28	2.4	180	40	5.68
0.4	200	533	1270	160	62.54	1.54	4.98	28	2.4	180	50	5.41
0.4	160	522	1270	160	62.54	1.54	4.98	28	2.4	180	60	5.16
0.34	400	649	1270	136	62.54	1.54	4.98	28	2.4	180	0	5.74
0.34	320	628	1270	136	62.54	1.54	4.98	28	2.4	180	20	6.07
0.34	280	618	1270	136	62.54	1.54	4.98	28	2.4	180	30	6.2
0.34	240	607	1270	136	62.54	1.54	4.98	28	2.4	180	40	6.2
0.34	200	596	1270	136	62.54	1.54	4.98	28	2.4	180	50	5.77
0.34	160	586	1270	136	62.54	1.54	4.98	28	2.4	180	60	5.17
0.3	400	692	1270	120	62.54	1.54	4.98	28	2.4	180	0	6.49
0.3	320	671	1270	120	62.54	1.54	4.98	28	2.4	180	20	6.6

0.3	280	660	1270	120	62.54	1.54	4.98	28	2.4	180	30	6.66
0.3	240	650	1270	120	62.54	1.54	4.98	28	2.4	180	40	6.71
0.3	200	639	1270	120	62.54	1.54	4.98	28	2.4	180	50	5.95
0.3	160	628	1270	120	62.54	1.54	4.98	28	2.4	180	60	5.45
0.4	400	585	1270	160	62.54	1.54	4.98	28	2.4	256	0	5.49
0.4	320	564	1270	160	62.54	1.54	4.98	28	2.4	256	20	5.61
0.4	280	554	1270	160	62.54	1.54	4.98	28	2.4	256	30	5.64
0.4	240	543	1270	160	62.54	1.54	4.98	28	2.4	256	40	5.83
0.4	200	533	1270	160	62.54	1.54	4.98	28	2.4	256	50	5.59
0.4	160	522	1270	160	62.54	1.54	4.98	28	2.4	256	60	5.34
0.34	400	649	1270	136	62.54	1.54	4.98	28	2.4	256	0	6.11
0.34	320	628	1270	136	62.54	1.54	4.98	28	2.4	256	20	6.19
0.34	280	618	1270	136	62.54	1.54	4.98	28	2.4	256	30	6.33
0.34	240	607	1270	136	62.54	1.54	4.98	28	2.4	256	40	6.57
0.34	200	596	1270	136	62.54	1.54	4.98	28	2.4	256	50	6.32
0.34	160	586	1270	136	62.54	1.54	4.98	28	2.4	256	60	5.61
0.3	400	692	1270	120	62.54	1.54	4.98	28	2.4	256	0	6.93
0.3	320	671	1270	120	62.54	1.54	4.98	28	2.4	256	20	7.04
0.3	280	660	1270	120	62.54	1.54	4.98	28	2.4	256	30	7.08
0.3	240	650	1270	120	62.54	1.54	4.98	28	2.4	256	40	7.28
0.3	200	639	1270	120	62.54	1.54	4.98	28	2.4	256	50	6.67
0.3	160	628	1270	120	62.54	1.54	4.98	28	2.4	256	60	5.6
0.4	400	585	1270	160	62.54	1.54	4.98	28	2.4	365	0	5.74
0.4	320	564	1270	160	62.54	1.54	4.98	28	2.4	365	20	5.84
0.4	280	554	1270	160	62.54	1.54	4.98	28	2.4	365	30	5.96
0.4	240	543	1270	160	62.54	1.54	4.98	28	2.4	365	40	6.06
0.4	200	533	1270	160	62.54	1.54	4.98	28	2.4	365	50	5.84
0.4	160	522	1270	160	62.54	1.54	4.98	28	2.4	365	60	5.48
0.34	400	649	1270	136	62.54	1.54	4.98	28	2.4	365	0	6.27
0.34	320	628	1270	136	62.54	1.54	4.98	28	2.4	365	20	6.33
0.34	280	618	1270	136	62.54	1.54	4.98	28	2.4	365	30	6.54
0.34	240	607	1270	136	62.54	1.54	4.98	28	2.4	365	40	6.71
0.34	200	596	1270	136	62.54	1.54	4.98	28	2.4	365	50	6.43
0.34	160	586	1270	136	62.54	1.54	4.98	28	2.4	365	60	5.78
0.3	400	692	1270	120	62.54	1.54	4.98	28	2.4	365	0	7.06
0.3	320	671	1270	120	62.54	1.54	4.98	28	2.4	365	20	7.06

0.3	280	660	1270	120	62.54	1.54	4.98	28	2.4	365	30	7.39
0.3	240	650	1270	120	62.54	1.54	4.98	28	2.4	365	40	7.5
0.3	200	639	1270	120	62.54	1.54	4.98	28	2.4	365	50	7.4
0.3	160	628	1270	120	62.54	1.54	4.98	28	2.4	365	60	6.22
-	250	1285	555	218	57.55	2.1	6.5	25.16	-	28	0	23.1
-	200	1293	558	216	57.55	2.1	6.5	25.16	-	28	15	21.3
-	200	1266	547	219	57.55	2.1	6.5	25.16	-	28	25	22.4
-	200	1246	538	221	57.55	2.1	6.5	25.16	-	28	33	22.9
-	200	1225	529	224	57.55	2.1	6.5	25.16	-	28	42	22.7
-	200	1203	519	229	57.55	2.1	6.5	25.16	-	28	50	21.4
-	200	1184	511	232	57.55	2.1	6.5	25.16	-	28	58	20
-	300	1242	536	225	57.55	2.1	6.5	25.16	-	28	0	29.5
-	240	1251	540	223	57.55	2.1	6.5	25.16	-	28	15	27.1
-	240	1221	527	225	57.55	2.1	6.5	25.16	-	28	25	29.2
-	240	1195	516	228	57.55	2.1	6.5	25.16	-	28	33	29.6
-	240	1176	508	231	57.55	2.1	6.5	25.16	-	28	42	29.8
-	240	1146	495	236	57.55	2.1	6.5	25.16	-	28	50	28.5
-	240	1122	484	240	57.55	2.1	6.5	25.16	-	28	58	26.9
-	350	1197	517	232	57.55	2.1	6.5	25.16	-	28	0	35.7
-	280	1208	522	230	57.55	2.1	6.5	25.16	-	28	15	33
-	280	1174	507	232	57.55	2.1	6.5	25.16	-	28	25	35.6
-	280	1142	493	236	57.55	2.1	6.5	25.16	-	28	33	36.2
-	280	1114	481	240	57.55	2.1	6.5	25.16	-	28	42	36.5
-	280	1088	470	245	57.55	2.1	6.5	25.16	-	28	50	35.5
-	280	1058	457	249	57.55	2.1	6.5	25.16	-	28	58	33.6
-	400	1154	498	239	57.55	2.1	6.5	25.16	-	28	0	41.5
-	320	1159	501	237	57.55	2.1	6.5	25.16	-	28	15	39.3
-	320	1122	484	240	57.55	2.1	6.5	25.16	-	28	25	41.4
-	320	1096	473	243	57.55	2.1	6.5	25.16	-	28	33	42.5
-	320	1062	458	247	57.55	2.1	6.5	25.16	-	28	42	42.7
-	320	1032	446	251	57.55	2.1	6.5	25.16	-	28	50	41.2
-	320	1009	436	255	57.55	2.1	6.5	25.16	-	28	58	39.5
-	250	1285	555	218	57.55	2.1	6.5	25.16	-	180	0	26.6
-	200	1293	558	216	57.55	2.1	6.5	25.16	-	180	15	25
-	200	1266	547	219	57.55	2.1	6.5	25.16	-	180	25	26.7
-	200	1246	538	221	57.55	2.1	6.5	25.16	-	180	33	27.2

-	200	1225	529	224	57.55	2.1	6.5	25.16	-	180	42	27.1
-	200	1203	519	229	57.55	2.1	6.5	25.16	-	180	50	25.7
-	200	1184	511	232	57.55	2.1	6.5	25.16	-	180	58	24.2
-	300	1242	536	225	57.55	2.1	6.5	25.16	-	180	0	34.2
-	240	1251	540	223	57.55	2.1	6.5	25.16	-	180	15	32.2
-	240	1221	527	225	57.55	2.1	6.5	25.16	-	180	25	34.6
-	240	1195	516	228	57.55	2.1	6.5	25.16	-	180	33	35.3
-	240	1176	508	231	57.55	2.1	6.5	25.16	-	180	42	35.6
-	240	1146	495	236	57.55	2.1	6.5	25.16	-	180	50	34.2
-	240	1122	484	240	57.55	2.1	6.5	25.16	-	180	58	32.6
-	350	1197	517	232	57.55	2.1	6.5	25.16	-	180	0	41.4
-	280	1208	522	230	57.55	2.1	6.5	25.16	-	180	15	38.9
-	280	1174	507	232	57.55	2.1	6.5	25.16	-	180	25	42.2
-	280	1142	493	236	57.55	2.1	6.5	25.16	-	180	33	43.3
-	280	1114	481	240	57.55	2.1	6.5	25.16	-	180	42	43.4
-	280	1088	470	245	57.55	2.1	6.5	25.16	-	180	50	42.5
-	280	1058	457	249	57.55	2.1	6.5	25.16	-	180	58	40.8
-	400	1154	498	239	57.55	2.1	6.5	25.16	-	180	0	48
-	320	1159	501	237	57.55	2.1	6.5	25.16	-	180	15	46.3
-	320	1122	484	240	57.55	2.1	6.5	25.16	-	180	25	49.3
-	320	1096	473	243	57.55	2.1	6.5	25.16	-	180	33	50.7
-	320	1062	458	247	57.55	2.1	6.5	25.16	-	180	42	50.9
-	320	1032	446	251	57.55	2.1	6.5	25.16	-	180	50	49.7
-	320	1009	436	255	57.55	2.1	6.5	25.16	-	180	58	48.3
0.38	347	864	1039	132	-	-	-	-	-	28	0	59
0.31	157	827	1152	109	45.2	1.36	24.83	20.7	-	28	56	68
0.46	304	830	1.68	139	-	-	-	-	-	28	0	49
0.35	154	768	1129	123	45.2	1.36	24.83	20.7	-	28	56	52
0.38	152	772	698	130	45.2	1.36	24.83	20.7	-	28	56	26
0.39	153	755	609	136	45.2	1.36	24.83	20.7	-	28	56	21
0.38	153	757	726	131	45.2	1.36	24.83	20.7	-	28	56	31
0.33	154	645	1198	120	49.02	2.37	12.31	26.69	-	28	58	32
0.33	149	631	1173	118	49.02	2.37	12.31	26.69	-	28	58	38
0.33	152	645	1203	119	46.2	14.93	7.7	15.6	-	28	58	37
0.33	154	650	1209	120	46.38	19.34	7.38	15.32	-	28	58	37
0.33	152	638	1187	119	47.33	1.81	13.82	25.44	-	28	58	33

0.36	500	876	876	180	50.5	2.6	7.4	24.7	-	1	0	38
0.36	400	845	876	180	50.5	2.6	7.4	24.7	-	1	20	19
0.36	300	813	876	180	50.5	2.6	7.4	24.7	-	1	40	17
0.36	200	782	876	180	50.5	2.6	7.4	24.7	-	1	60	5
0.36	100	751	876	180	50.5	2.6	7.4	24.7	-	1	80	0
0.36	500	876	876	180	50.5	2.6	7.4	24.7	-	7	0	65
0.36	400	845	876	180	50.5	2.6	7.4	24.7	-	7	20	42
0.36	300	813	876	180	50.5	2.6	7.4	24.7	-	7	40	42
0.36	200	782	876	180	50.5	2.6	7.4	24.7	-	7	60	21.5
0.36	100	751	876	180	50.5	2.6	7.4	24.7	-	7	80	6
0.36	500	876	876	180	50.5	2.6	7.4	24.7	-	28	0	72
0.36	400	845	876	180	50.5	2.6	7.4	24.7	-	28	20	55
0.36	300	813	876	180	50.5	2.6	7.4	24.7	-	28	40	58
0.36	200	782	876	180	50.5	2.6	7.4	24.7	-	28	60	32.5
0.36	100	751	876	180	50.5	2.6	7.4	24.7	-	28	80	10
0.36	500	876	876	180	50.5	2.6	7.4	24.7	-	56	0	85
0.36	400	845	876	180	50.5	2.6	7.4	24.7	-	56	20	61
0.36	300	813	876	180	50.5	2.6	7.4	24.7	-	56	40	69
0.36	200	782	876	180	50.5	2.6	7.4	24.7	-	56	60	39
0.36	100	751	876	180	50.5	2.6	7.4	24.7	-	56	80	12
0.35	404	570	353	202	59.18	2.38	8.8	22.8	2.3	3	30	24
0.35	404	570	353	202	59.18	2.38	8.8	22.8	2.3	3	30	30
0.35	404	570	353	202	59.18	2.38	8.8	22.8	2.3	3	30	30
0.3	333	545	338	200	59.18	2.38	8.8	22.8	2.3	3	50	15
0.3	333	545	338	193	59.18	2.38	8.8	22.8	2.3	3	50	23
0.3	333	545	338	195	59.18	2.38	8.8	22.8	2.3	3	50	23
0.35	404	570	353	202	59.18	2.38	8.8	22.8	2.3	7	30	32
0.35	404	570	353	202	59.18	2.38	8.8	22.8	2.3	7	30	39
0.35	404	570	353	202	59.18	2.38	8.8	22.8	2.3	7	30	40
0.3	333	545	338	200	59.18	2.38	8.8	22.8	2.3	7	50	19
0.3	333	545	338	193	59.18	2.38	8.8	22.8	2.3	7	50	32
0.3	333	545	338	195	59.18	2.38	8.8	22.8	2.3	7	50	32
0.35	404	570	353	202	59.18	2.38	8.8	22.8	2.3	28	30	49
0.35	404	570	353	202	59.18	2.38	8.8	22.8	2.3	28	30	53
0.35	404	570	353	202	59.18	2.38	8.8	22.8	2.3	28	30	57.5
0.3	333	545	338	200	59.18	2.38	8.8	22.8	2.3	28	50	22

0.3	333	545	338	193	59.18	2.38	8.8	22.8	2.3	28	50	42
0.3	333	545	338	195	59.18	2.38	8.8	22.8	2.3	28	50	49
0.42	202.4	707.5	1057.3	180.4	33.1	28.5	6.53	11.6	2.37	3	60	10
0.42	201.9	707.5	1057.3	180.7	55.8	5.87	8.31	21	2.39	3	60	7
0.42	202.4	707.5	0	180.4	33.1	28.5	6.53	11.6	2.37	3	60	4
0.42	201.9	707.5	0	180.7	55.8	5.87	8.31	21	2.39	3	60	3
0.42	202.4	707.5	1057.3	180.4	33.1	28.5	6.53	11.6	2.37	28	60	34
0.42	201.9	707.5	1057.3	180.7	55.8	5.87	8.31	21	2.39	28	60	24
0.42	202.4	707.5	0	180.4	33.1	28.5	6.53	11.6	2.37	28	60	24
0.42	201.9	707.5	0	180.7	55.8	5.87	8.31	21	2.39	28	60	11
0.42	202.4	707.5	1057.3	180.4	33.1	28.5	6.53	11.6	2.37	90	60	46
0.42	201.9	707.5	1057.3	180.7	55.8	5.87	8.31	21	2.39	90	60	31
0.42	202.4	707.5	0	180.4	33.1	28.5	6.53	11.6	2.37	90	60	37
0.42	201.9	707.5	0	180.7	55.8	5.87	8.31	21	2.39	90	60	17
0.75	255	1745	-	190	47.8	7.1	3.8	30.7	-	3	0	10.5
0.49	385	1680	-	190	47.8	7.1	3.8	30.7	-	3	0	23.5
0.37	510	1675	-	190	47.8	7.1	3.8	30.7	-	3	0	39
0.7	215	1970	-	175	47.8	7.1	3.8	30.7	-	3	15	10.5
0.45	330	1850	-	175	47.8	7.1	3.8	30.7	-	3	15	23
0.35	420	1740	-	175	47.8	7.1	3.8	30.7	-	3	15	38.5
0.63	190	1950	-	170	47.8	7.1	3.8	30.7	-	3	30	10
0.41	290	1820	-	170	47.8	7.1	3.8	30.7	-	3	30	23
0.33	360	1700	-	170	47.8	7.1	3.8	30.7	-	3	30	38
0.53	170	1925	-	165	47.8	7.1	3.8	30.7	-	3	45	9.5
0.24	270	1755	-	165	47.8	7.1	3.8	30.7	-	3	45	21.5
0.36	350	1545	-	165	47.8	7.1	3.8	30.7	-	3	45	33.5
0.75	255	1745	-	190	47.8	7.1	3.8	30.7	-	7	0	16.5
0.49	385	1680	-	190	47.8	7.1	3.8	30.7	-	7	0	34.5
0.37	510	1675	-	190	47.8	7.1	3.8	30.7	-	7	0	52.5
0.7	215	1970	-	175	47.8	7.1	3.8	30.7	-	7	15	16
0.45	330	1850	-	175	47.8	7.1	3.8	30.7	-	7	15	33
0.35	420	1740	-	175	47.8	7.1	3.8	30.7	-	7	15	51
0.63	190	1950	-	170	47.8	7.1	3.8	30.7	-	7	30	15
0.41	290	1820	-	170	47.8	7.1	3.8	30.7	-	7	30	32
0.33	360	1700	-	170	47.8	7.1	3.8	30.7	-	7	30	48
0.53	170	1925	-	165	47.8	7.1	3.8	30.7	-	7	45	14

0.24	270	1755	-	165	47.8	7.1	3.8	30.7	-	7	45	30
0.36	350	1545	-	165	47.8	7.1	3.8	30.7	-	7	45	45
0.75	255	1745	-	190	47.8	7.1	3.8	30.7	-	14	0	20.5
0.49	385	1680	-	190	47.8	7.1	3.8	30.7	-	14	0	41.5
0.37	510	1675	-	190	47.8	7.1	3.8	30.7	-	14	0	62.5
0.7	215	1970	-	175	47.8	7.1	3.8	30.7	-	14	15	20
0.45	330	1850	-	175	47.8	7.1	3.8	30.7	-	14	15	40.5
0.35	420	1740	-	175	47.8	7.1	3.8	30.7	-	14	15	62.5
0.63	190	1950	-	170	47.8	7.1	3.8	30.7	-	14	30	19.5
0.41	290	1820	-	170	47.8	7.1	3.8	30.7	-	14	30	40
0.33	360	1700	-	170	47.8	7.1	3.8	30.7	-	14	30	57.5
0.53	170	1925	-	165	47.8	7.1	3.8	30.7	-	14	45	18.5
0.24	270	1755	-	165	47.8	7.1	3.8	30.7	-	14	45	39
0.36	350	1545	-	165	47.8	7.1	3.8	30.7	-	14	45	55.5
0.4	352	676	1205	141	50.96	2.15	8.25	25.88	-	3	0	24.23
0.4	282	676	1205	141	50.96	2.15	8.25	25.88	-	3	20	16.95
0.4	246	675	1205	141	50.96	2.15	8.25	25.88	-	3	30	14.23
0.4	352	676	1205	141	50.96	2.15	8.25	25.88	-	7	0	33.18
0.4	282	676	1205	141	50.96	2.15	8.25	25.88	-	7	20	30.12
0.4	246	675	1205	141	50.96	2.15	8.25	25.88	-	7	30	30.06
0.4	352	676	1205	141	50.96	2.15	8.25	25.88	-	28	0	47.51
0.4	282	676	1205	141	50.96	2.15	8.25	25.88	-	28	20	48.96
0.4	246	675	1205	141	50.96	2.15	8.25	25.88	-	28	30	45.1
0.4	352	676	1205	141	50.96	2.15	8.25	25.88	-	90	0	55.13
0.4	282	676	1205	141	50.96	2.15	8.25	25.88	-	90	20	59.35
0.4	246	675	1205	141	50.96	2.15	8.25	25.88	-	90	30	55.11
0.4	352	676	1205	141	50.96	2.15	8.25	25.88	-	180	0	57.22
0.4	282	676	1205	141	50.96	2.15	8.25	25.88	-	180	20	62.81
0.4	246	675	1205	141	50.96	2.15	8.25	25.88	-	180	30	58.83
0.4	352	676	1205	141	50.96	2.15	8.25	25.88	-	365	0	59.25
0.4	282	676	1205	141	50.96	2.15	8.25	25.88	-	365	20	67.29